



Article

# Thermodynamic Theory of Phase Separation in Nonstoichiometric Si Oxide Films Induced by High-Temperature Anneals

Andrey Sarikov

V. Lashkaryov Institute of Semiconductor Physics NAS Ukraine, 41 Nauky Avenue, 03028 Kyiv, Ukraine; sarikov@isp.kiev.ua

**Abstract:** High-temperature anneals of nonstoichiometric Si oxide ( $\text{SiO}_x$ ,  $x < 2$ ) films induce phase separation in them, with the formation of composite structures containing amorphous or crystalline Si nanoinclusions embedded in the Si oxide matrix. In this paper, a thermodynamic theory of the phase separation process in  $\text{SiO}_x$  films is proposed. The theory is based on the thermodynamic models addressing various aspects of this process which we previously developed. A review of these models is provided, including: (i) the derivation of the expressions for the Gibbs free energy of Si oxides and Si/Si oxide systems, (ii) the identification of the phase separation driving forces and counteracting mechanisms, and (iii) the crystallization behavior of amorphous Si nanoinclusions in the Si oxide matrix. A general description of the phase separation process is presented. A number of characteristic features of the nano-Si/Si oxide composites formed by  $\text{SiO}_x$  decomposition, such as the local separation of Si nanoinclusions surrounded by the Si oxide matrix; the dependence of the amount of separated Si and the equilibrium matrix composition on the initial Si oxide stoichiometry and annealing temperature; and the correlation of the presence of amorphous and crystalline Si nanoinclusions with the presence of  $\text{SiO}_x$  ( $x < 2$ ) and  $\text{SiO}_2$  phase, respectively, in the Si oxide matrix, are explained.

**Keywords:** thermodynamic theory; phase separation; nonstoichiometric Si oxide; Gibbs free energy; Si nanoparticles; penalty energy; stress; crystallization; thermodynamic equilibrium



**Citation:** Sarikov, A. Thermodynamic Theory of Phase Separation in Nonstoichiometric Si Oxide Films Induced by High-Temperature Anneals. *Nanomanufacturing* **2023**, *3*, 293–314. <https://doi.org/10.3390/nanomanufacturing3030019>

Academic Editor: Ana María Díez-Pascual

Received: 1 May 2023

Revised: 5 June 2023

Accepted: 25 June 2023

Published: 3 July 2023



**Copyright:** © 2023 by the author. Licensee MDPI, Basel, Switzerland. This article is an open access article distributed under the terms and conditions of the Creative Commons Attribution (CC BY) license (<https://creativecommons.org/licenses/by/4.0/>).

## 1. Introduction

The high-temperature phase separation of nonstoichiometric Si oxide ( $\text{SiO}_x$ ,  $x < 2$ ) films is a key method for producing composite structures consisting of nanosized Si (nano-Si) inclusions embedded in a Si oxide matrix, for Si-based nanoelectronic device applications. In particular, nano-Si/Si oxide composites are proposed for use in light emitting devices [1,2], flash memory floating gates [3,4], photodiodes [5,6], electron field emission cathodes [7,8], and solar cells [9,10]. The possibilities of extending the optical, luminescence, and electrical properties of such composites are sought by modifying them with such metals as Er [11], Sn [12], Sm [13], Fe [14], and Al [15].

Various methods, such as Si ion implantation in  $\text{SiO}_2$  [16], sputtering [17] and electron beam evaporation [18,19] of Si and SiO, plasma-enhanced chemical vapor deposition [20,21], magnetron sputtering [22], and the thermal vacuum or reactive evaporation of SiO [23,24] are used in fabricating  $\text{SiO}_x$  films. The average size of the Si nanoparticles formed as a result of phase separation can be controlled by varying the annealing temperature, or by tuning the initial Si oxide composition. A reduction in oxygen content in the  $\text{SiO}_x$  films leads to an increase in the nano-Si size and density, and the standard deviation of their distribution [25,26]. Raising the annealing temperature also results in an increase in the average nano-Si size [27,28]. A higher level of flexibility is provided by the superlattice approach proposed by Zacharias et al. [29], in which thin  $\text{SiO}_x$  layers alternate with stoichiometric  $\text{SiO}_2$  layers not undergoing separation, thus enabling an independent control of

the location, size (corresponding to the SiO<sub>x</sub> layer thickness), and concentration of the Si nanoinclusions in the Si oxide matrix.

During high-temperature annealing, the partial or complete decomposition of nonstoichiometric Si oxide takes place, according to the following reaction:



where  $x_0$  and  $x$  are the initial and the current stoichiometry indexes of the Si oxide phase, respectively. The reaction (1) leads to the separation of Si nanoparticles, and an increase in oxygen concentration in the surrounding Si oxide matrix.

The degree of phase separation in SiO<sub>x</sub> films is often characterized by the equilibrium stoichiometry index of the Si oxide matrix,  $x_{eq}$ , which also indicates the amount of separated Si and, hence, the concentration and the average size of formed Si nanoinclusions. Experimental data show that  $x_{eq} < 2$  (incomplete separation) for annealing temperatures below about 950 °C, and increases with the increase in both  $x_0$  and  $T$  [30–32]. The degree of phase separation correlates with the amorphous or crystalline state of Si nanoinclusions. For annealing temperatures not exceeding approximately 950 °C, mainly amorphous Si (a-Si) nanoparticles form, while at higher temperatures, the formation of Si nanocrystallites takes place, as revealed by Raman scattering, infrared (IR) absorption, x-ray photoelectron spectroscopy (XPS), and high-resolution electron microscopy investigations [24,33,34].

Understanding the phase separation phenomenon in SiO<sub>x</sub> films in terms of thermodynamics would enable the unveiling of its mechanisms, as well as laying the foundation for the macroscopic description of its kinetics. A thermodynamic approach requires knowledge about transformations of the Gibbs free energy in Si/Si oxide systems during high-temperature anneals. The minimum values of the Gibbs free energy determine the equilibrium between the separated Si and Si oxide phases, as well as the equilibrium Si oxide composition.

A literature review demonstrates that studies aimed at the thermodynamic description of phase separation in nonstoichiometric Si oxide films are practically absent. A limited number of papers [35,36] present thermodynamic analyses of Si–O systems, with emphasis on particular compositions such as Si<sub>2</sub>O<sub>3</sub>, SiO, and Si<sub>2</sub>O, as well as different SiO<sub>2</sub> phases. To our best knowledge, the only recent attempt to phenomenologically introduce the Gibbs free energy of a nonstoichiometric Si oxide was undertaken by La Magna et al. [37], to describe the mechanism of the incomplete separation of the SiO<sub>x</sub> phase, and its dependence on the initial Si oxide stoichiometry. The thermodynamically derived expression for the Gibbs free energy of Si oxide and Si/Si oxide systems was first presented in our publication [38]. By analyzing transformations of the Gibbs free energy with the annealing temperature and the amount of separated Si, the formation of equilibrium between bulk amorphous or crystalline Si and Si oxide was studied in detail. The thermodynamic model of equilibrium states in Si/Si oxide systems was later modified, to take into account other aspects of the phase separation process, such as the influence of stress [39,40] and nano-Si/Si oxide interfaces [41,42], and the crystallization behavior of amorphous Si nanoinclusions embedded in a Si oxide matrix [43].

In this paper, we review the theoretical models that we developed earlier, which constitute the general thermodynamic theory of phase separation in nonstoichiometric Si oxide films. The formation of nano-Si/Si oxide composites by high-temperature SiO<sub>x</sub> decomposition is discussed in the framework of this theory, simultaneously taking into account various aspects of the phase separation process. A number of the characteristic features of this process, and the formed nano-Si/Si oxide composites, are explained, including: (i) the mechanism of the local separation of the Si phase, accompanied by a homogeneous increase in the stoichiometry index of the Si oxide matrix, (ii) the dependence of the amount of separated Si and the equilibrium matrix composition on the initial Si oxide stoichiometry and annealing temperature, and (iii) the correlation of the presence of amorphous Si nanoinclusions with the SiO<sub>x</sub> ( $x < 2$ ) phase, and crystalline Si inclusions with the SiO<sub>2</sub> phase, in the Si oxide matrix. The proposed general thermodynamic theory may be further used as a

basis for developing kinetic models, which will enable the optimization of technologies in the formation of nano-Si/Si oxide composites for a broad range of applications.

## 2. Theory and Results

As already mentioned in the Introduction section, the thermodynamic theory of phase separation in nonstoichiometric Si oxide films, induced by high-temperature anneals, integrates a number of theoretical models considered in our previous publications [38–43]. The subjects of these models are listed in the left-hand side of the diagram shown in Figure 1. Such integration will provide a deeper understanding of the  $\text{SiO}_x$  phase separation phenomenon in terms of thermodynamics, as is schematically shown in the central part of the diagram in Figure 1. The unified theory will enable us to predict the state of nano-Si/Si oxide composites (the quantity of separated Si, the equilibrium stoichiometry of the Si oxide matrix, the amorphous or crystalline state of Si nano-inclusions, etc.) as a function of the initial Si oxide composition and annealing conditions. Its different components have already been successfully applied to reveal the kinetic mechanisms of phase separation [44]; understand the annealing-induced transformations in Si oxide, oxynitride and nitride-based superlattices with nanometer thick layers [45–49]; and describe the structural properties of Si oxynitrides grown at different temperatures [50], as depicted in the right-hand side of the diagram presented in Figure 1. All the theoretical models composing the unified thermodynamic theory are reviewed below, followed by a general discussion of the phase separation process in  $\text{SiO}_x$  films, in the Discussion section.

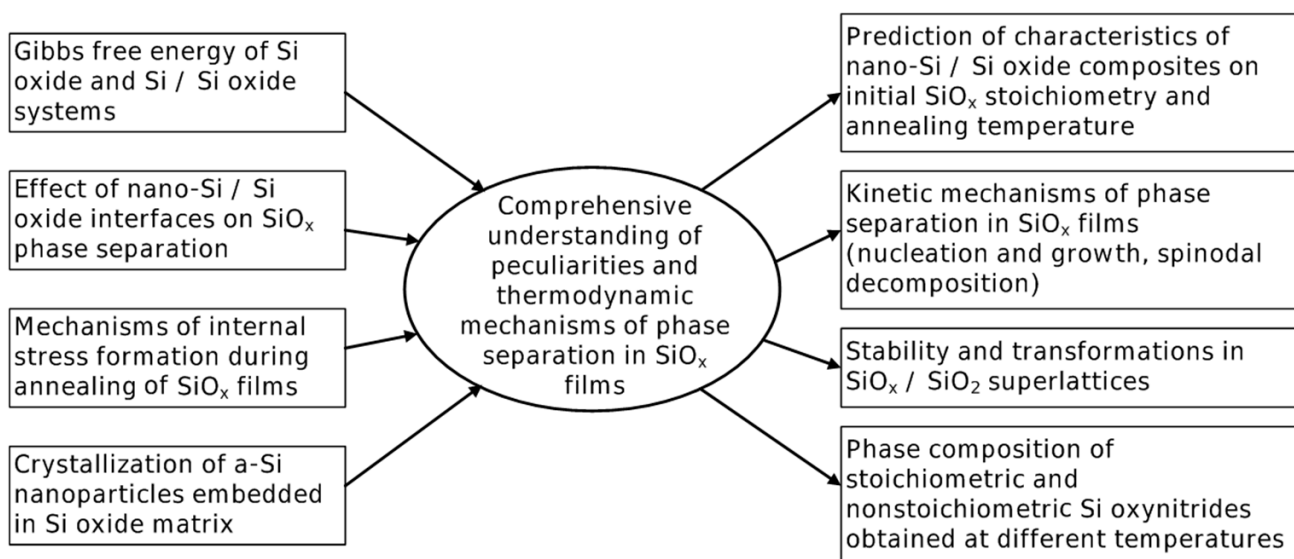


**Figure 1.** Diagram of the components and application areas of the thermodynamic theory of phase separation in  $\text{SiO}_x$  films.

### 2.1. Gibbs Free Energy of Si/Si Oxide Systems

The key issue in the thermodynamic theory of phase separation in  $\text{SiO}_x$  films is obtaining the Gibbs free energy of the Si oxides and Si/Si oxide systems. The method of deriving the Gibbs free energy of the mentioned systems, as well as the results of the study of equilibrium between the contacting Si and Si oxide phases, was described in detail in our previous publication [38]. According to the method used there, the temperature-induced separation of excess Si atoms from Si oxide with the initial stoichiometry  $x_0$  is considered according to the reaction (1) until the equilibrium stoichiometry  $x = x_{eq}$ , corresponding to the minimum Gibbs free energy of the resulting Si/Si oxide system, is achieved. As a first approximation, contacting planar Si and  $\text{SiO}_x$  layers shown schematically in Figure 2 are assumed to form by  $\text{SiO}_{x0}$  decomposition, instead of experimentally observed nano-Si inclusions distributed within the Si oxide matrix. Such approximation enables us to ignore

the contribution to the Gibbs free energy from the interfaces between the nano-Si inclusions and the surrounding matrix. Moreover, the separation of Si in the amorphous state is considered in the most general case, Si oxide and crystalline Si (c-Si)/Si oxide systems being the partial cases.

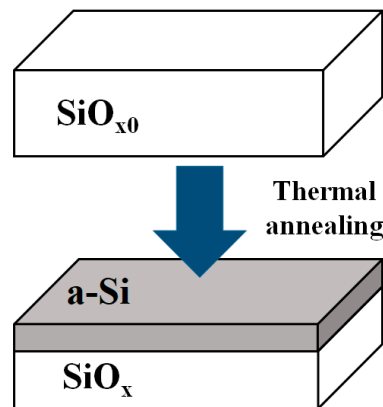


**Figure 2.** Geometry of the initial  $\text{SiO}_{x_0}$  phase, and phase separated a-Si/Si oxide system.

The following provisions establish the background for deriving the expression for the Gibbs free energy of Si oxides and Si/Si oxide systems [38]:

1. The Gibbs free energy of the a-Si phase is expressed in terms of the Gibbs free energy of c-Si plus the excess energy equal to  $\Delta g_{ac} = \frac{h_E - s_E T}{N_A}$  per one Si atom [51]. Here,  $h_E = 13,400$  J/mole is the molar crystallization enthalpy [52],  $s_E = 3.97$  J/mole  $\times$  K is the molar excess entropy of amorphous-to-crystalline transition [53], and  $N_A = 6.022 \times 10^{23}$  mole $^{-1}$  is the Avogadro constant, respectively.
2. The nonstoichiometric Si oxide phase is considered in the binary solution approximation [54], in which the  $\text{SiO}_x$  solution is formed by mixing elemental Si and oxygen atoms obtained by the decomposition of  $\text{O}_2$  molecules.
3. The structure of Si oxide is made up of interconnected  $\text{Si-O}_y\text{Si}_{4-y}$  tetrahedral units ( $0 \leq y \leq 4$ ) with different oxidation degrees  $y$  of a central Si atom. In addition to the Si-Si and Si-O bond energies, each tetrahedral unit is characterized by the penalty energy  $\Delta_y$  as the measure of the energy nonequivalence of the units with different values of  $y$  ( $\Delta_0 = \Delta_4 = 0$  eV,  $\Delta_1 = 0.5$  eV,  $\Delta_2 = 0.51$  eV, and  $\Delta_3 = 0.22$  eV) [55]. The probability of finding a tetrahedral unit with either value of  $y$  obeys the random bonding model proposed by Phillip [56].
4. The entropy of mixing is considered to be the configuration entropy of the Si oxide phase, associated with the number of arrangements of oxygen atoms between the pairs of Si atoms.

As demonstrated in [38], the Gibbs free energy of an a-Si/Si oxide system is conveniently expressed per one atom in this system, which naturally provides its dependence on the initial and current stoichiometry indexes of the Si oxide phase,  $x_0$  and  $x$ , respectively, and the annealing temperature, as the variables:

$$g(x_0, x, T) = \frac{x_0}{1+x_0} \left\{ \frac{1}{x} \sum_{y=0}^4 \frac{4!}{(4-y)!y!} \left(\frac{x}{2}\right)^y \left[\frac{2-x}{2}\right]^{4-y} \Delta_y - kT \left( \frac{2}{x} \ln \frac{2}{2-x} - \ln \frac{x}{2-x} \right) - \frac{1}{x} \frac{h_E - s_E T}{N_A} \right\} \quad (2)$$

where  $k = 1.38 \times 10^{-23}$  J/K is the Boltzmann's constant. In deriving the expression (2), all the contributions which are not the functions of  $(x_0, x, T)$  were omitted, as they have no influence on determining the equilibrium states in Si/Si oxide systems. The first term between the braces is the part of the mixing enthalpy corresponding to the total penalty

energy of all the  $\text{Si-O}_y\text{Si}_{4-y}$  tetrahedral units composing the Si oxide matrix. The second term is the configuration entropy contribution, and the only one that is temperature-dependent. The third term expresses the excess Gibbs free energy of a-Si, as compared to that of c-Si. The expression (2) can be modified to provide the Gibbs free energy of other considered systems. In particular, the truncation of the term proportional to the  $\frac{h_E - s_E T}{N_A}$  results in the Gibbs free energy per one atom of a c-Si/Si oxide system, while setting additionally  $x = x_0$ , turns it into the Gibbs free energy of the Si oxide phase.

Each term between the braces in the expression (2) corresponds to a single mechanism, which drives or counteracts the separation of the initial nonstoichiometric Si oxide into Si and  $\text{SiO}_x$  phases, depending on whether it is a descending or ascending function of  $x$ . The mathematical analysis shows that the only driving force for demixing is the tendency to decrease the total penalty energy of all the  $\text{Si-O}_y\text{Si}_{4-y}$  tetrahedral units, which has zero value for the coexisting stoichiometric Si and  $\text{SiO}_2$  phases (only Si-Si<sub>4</sub> and Si-O<sub>4</sub> tetrahedra with  $\Delta_0 = \Delta_4 = 0$ ). The phase separation is counteracted by the formation of the amorphous Si phase (in the case of a-Si/Si oxide systems), as well as by the decrease in the configuration entropy, with the increase in  $x$  leading to the increase in the respective Gibbs free energy contribution. As a result, the equilibrium between the Si and Si oxide phases is predicted at some value  $x_{eq} < 2$ , which may be interpreted in terms of the solubility limit of Si in  $\text{SiO}_2$  [38].

The application of the expression (2) provides a description of equilibrium states in bulk Si/Si oxide systems. The calculated dependences of the Gibbs free energy on  $x$  for different temperatures and values of  $x_0$  are shown in Figure 3a,b, respectively. The minima of the curves correspond to the equilibrium between the Si and Si oxide phases. It can be seen from Figure 3a,c that  $x_{eq}$  is predicted not to depend on the initial Si excess (value of  $x_0$ ), which is also supported by the mathematical analysis of the expression (2) [38]. Moreover,  $x_{eq}$  in the described model decreases with annealing temperature (see Figure 3b,d), which corresponds to the increase in the concentration of the Si dissolved in  $\text{SiO}_2$ , in full consistency with the Si solubility concept. However, such findings contradict the experimental observations of phase separation in  $\text{SiO}_x$  films, with the formation of nanosized Si inclusions in the Si oxide matrix. According to these observations, the equilibrium Si oxide stoichiometry increases with both  $x_0$  and annealing temperature [30–32]. Hence, the expression (2) should be modified, by taking into account additional mechanisms, to describe the experimental dependences of  $x_{eq}$ . These mechanisms and their effects on the equilibrium in nano-Si/Si oxide systems are discussed in the next sections.

## 2.2. Effect of Nano-Si/Si Oxide Matrix Interfaces on Phase Equilibria in Si/Si Oxide Systems

One of the mechanisms that might have an influence on phase separation in  $\text{SiO}_x$  films is the formation of interfaces of nano-Si inclusions with the surrounding Si oxide matrix. The total relative area of such interfaces is high enough in view of the small nano-Si sizes and their high concentrations. The interface-related contribution to the Gibbs free energy (2) is positive. Therefore, there is a need to verify the effect of the interface free energy on the value of  $x_{eq}$  and its dependence on the annealing temperature.

The effect of the interfaces between the nano-Si inclusions and the Si oxide matrix is described in [41,42]. For simplicity, Si nano-inclusions with equal radii  $R$  are considered. The radius  $R$  is calculated as follows:

$$R = \sqrt[3]{\frac{3\Omega}{4\pi} i} = \sqrt[3]{\frac{3\Omega}{4\pi} \frac{x - x_0}{x(1 + x_0)} \frac{C_0}{C_{incl}}} \quad (3)$$

where  $\Omega \approx 2.29 \times 10^{-29} \text{ m}^3$  is the atomic volume of Si [57],  $i$  is the quantity of Si atoms in a single nano-inclusion,  $C_0 = 7 \times 10^{22} \text{ cm}^{-3}$  is accepted to be the total atomic concentration of the  $\text{SiO}_x$  phase [37], and  $C_{incl} \sim 10^{18}\text{--}10^{19} \text{ cm}^{-3}$  is the typical concentration of Si nano-inclusions formed as a result of phase separation [58,59], respectively.  $R$  is directly related to the concentration of separated Si, which is expressed as  $\frac{x - x_0}{x(1 + x_0)} C_0$ .

The interface contribution to the Gibbs free energy per one atom for a nano-Si inclusion embedded in Si oxide looks as follows:

$$g_{interface} = 4\pi\gamma_{oa}R^2\frac{C_{incl}}{C_0} \quad (4)$$

where  $\gamma_{oa}$  is the specific interface energy of nano-Si/Si oxide interface. Since the analysis is carried out for the temperature range of incomplete phase separation, which implies the predominant formation of a-Si nanoinclusions [24,33,34],  $\gamma_{oa} = 0.01 \text{ J/m}^2$  is set corresponding to the a-Si/SiO<sub>2</sub> interface [43].

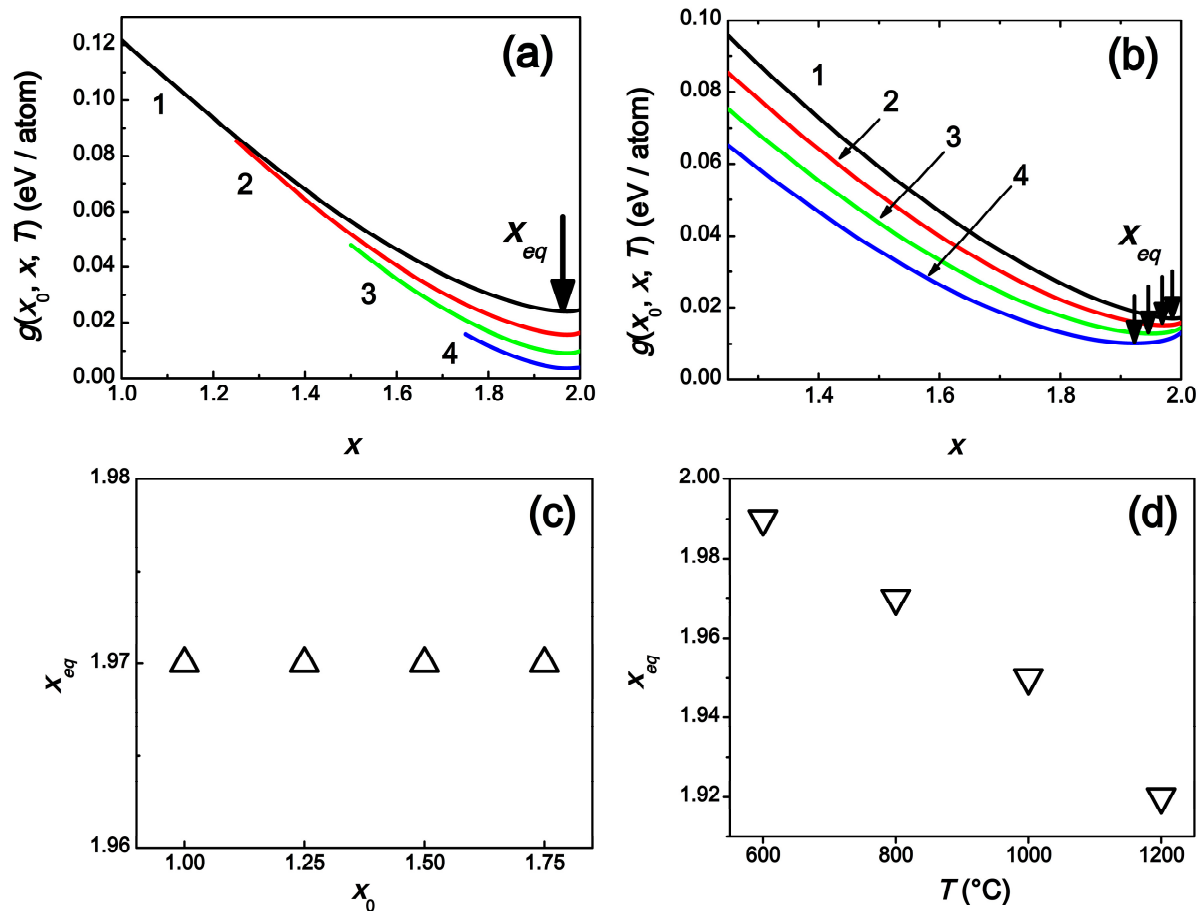


**Figure 3.** The dependence of the Gibbs free energy per one atom on the stoichiometry index of Si oxide in the a-Si/Si oxide systems, calculated by the expression (2). (a) For different initial Si oxide stoichiometry indexes,  $x_0$ : 1—1, 2—1.25, 3—1.5, and 4—1.75. The annealing temperature  $T = 800^\circ\text{C}$ . (b) For different annealing temperatures,  $T$ : 1—600, 2—800, 3—1000, and 4—1200  $^\circ\text{C}$ . The initial Si oxide stoichiometry  $x_0 = 1.25$ . The arrows in the panels indicate equilibrium stoichiometry indexes of the Si oxide phase. All the curves are shifted by  $\frac{1}{1+x_0} \frac{hF - sET}{N_A}$  for better visualization. Panels (c) and (d) show the equilibrium stoichiometry index of Si oxide versus its initial stoichiometry and annealing temperature, recalculated using the data presented in panels (a) and (b), respectively.

Figure 4 shows the dependences of  $g_{interface}$  calculated by the expression (4) on the stoichiometry index of the SiO<sub>x</sub> matrix for different initial Si oxide stoichiometries  $x_0$  and nano-Si concentrations. It can be seen from this figure that the contributions of a-Si/Si oxide interfaces to the Gibbs free energy do not exceed approximately  $5 \times 10^{-4} \text{ eV/atom}$  for reasonable  $C_{incl}$  values, which is at least two orders of magnitude smaller than the data presented in Figure 3a,b. The partial crystallization of amorphous Si nanoinclusions may lead to the modification of  $\gamma_{oa}$  by about one order of magnitude (the specific energy of

the bulk c-Si/SiO<sub>2</sub> interface ranges from 0.1 to 0.6 J/m<sup>2</sup> [60,61]), which will result in the proportional change in the interface contribution to the Gibbs free energy. However, no significant modification in the Gibbs free energy expressed as the sum of (2) and (4) will be achieved. Moreover, multiple studies have demonstrated that the interface free energy of nanoparticles decreases upon reducing their sizes [62,63], which leads to an even smaller contribution to the Gibbs free energy from the nano-Si/Si oxide interfaces. Therefore, the role of the mentioned interfaces on equilibrium states in Si/Si oxide systems during phase separation in SiO<sub>x</sub> films may be considered insignificant, and therefore ignored in further analysis.

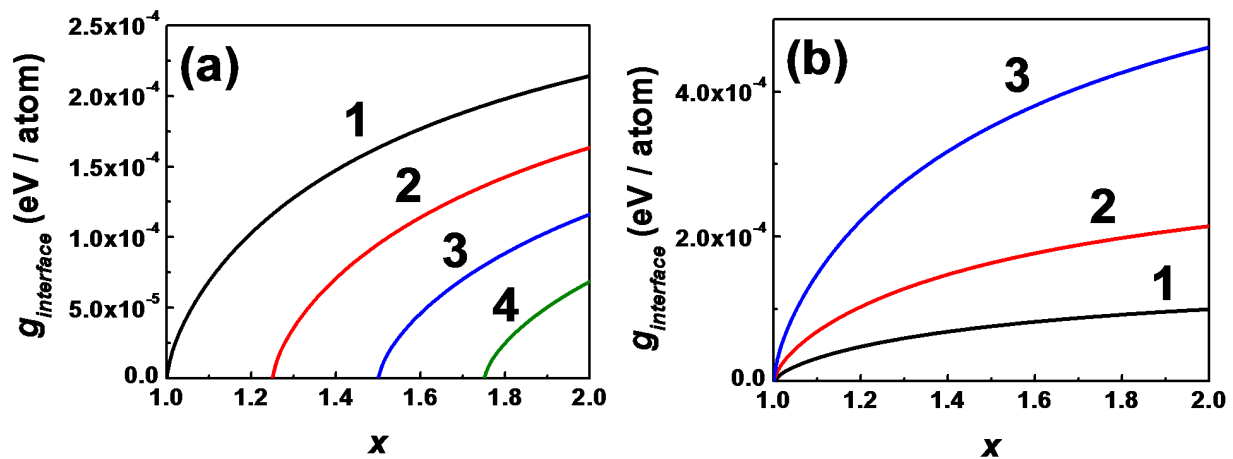


**Figure 4.** The dependence of the interface contribution to the Gibbs free energy of a-Si/SiO<sub>x</sub> system on the stoichiometry index of the Si oxide phase. (a) For different initial Si oxide stoichiometries,  $x_0$ : 1—1, 2—1.25, 3—1.5, and 4—1.75. The concentration of the Si nanoinclusions  $C_{incl} = 10^{18} \text{ cm}^{-3}$ . (b) For different concentrations of Si nanoinclusions,  $C_{incl}$ : 1— $10^{17}$ , 2— $10^{18}$ , and 3— $10^{19} \text{ cm}^{-3}$ . The initial Si oxide stoichiometry  $x_0 = 1$ .

### 2.3. Influence of Internal Stress on Phase Separation in SiO<sub>x</sub> Films

The formation of internal stress during the phase decomposition of SiO<sub>x</sub> films was found to be key to define the equilibrium between the separated Si and Si oxide phases. The mathematical form of the stress-related contribution to the Gibbs free energy of Si/Si oxide systems was proposed in our earlier publication [39], and its parameters were determined by comparing the theoretical predictions with the experimental dependences of  $x_{eq}$  on the annealing temperature. Here, we briefly review the main results obtained in [39], as required for the further general analysis of the phase separation process in nonstoichiometric Si oxides. The possible mechanisms of the formation of internal stress are discussed in the Discussion section.

The formation of equilibrium states during the phase separation of SiO<sub>x</sub> films under the action of internal stress was studied using the extended expression (2) for the Gibbs free energy per one atom:

$$g(x_0, x, T) = \frac{x_0}{1+x_0} \left\{ \frac{1}{x} \sum_{y=0}^4 \frac{4!}{(4-y)!y!} \left(\frac{x}{2}\right)^y \left[\frac{2-x}{2}\right]^{4-y} \Delta_y - kT \left( \frac{2}{x} \ln \frac{2}{2-x} - \ln \frac{x}{2-x} \right) - \frac{1}{x} \frac{h_{E-S} T}{N_A} \right\} + \chi(T)(x - x_0)^2 \quad (5)$$

where the last term is the stress-related Gibbs free energy contribution obtained by modifying the respective expression proposed in [37] with the temperature-dependent function  $\chi(T)$ . The mathematical form of this term fully complies with the requirements set up in [39], to enable the agreement of the theoretical and experimental dependences of the equilibrium stoichiometry of Si oxides on their initial composition and annealing temperature, namely:

1. the superlinear dependence on the difference between the current and the initial Si oxide stoichiometry indexes, to be able to reproduce the increase in the value of  $x_{eq}$  with the increase in  $x_0$ ;
2. the descending dependence on the annealing temperature, to enable the minimum Gibbs free energy of a Si/Si oxide system shift toward smaller  $x$ , upon raising the temperature.

The values of the function  $\chi(T)$  were found by comparing the values of  $x_{eq}$  calculated from the minimum condition of the expression (5), with the corresponding experimental saturation stoichiometry indexes of the Si oxide matrix obtained after anneals of  $\text{SiO}_x$  films at different temperatures. We present here only the results obtained for the thermal vacuum sputtered  $\text{SiO}_{1.25}$  films [31]. The experimental dependence of the equilibrium stoichiometry index on the annealing temperature for these films is shown in Figure 5a, while Figure 5b provides, by symbols, the corresponding values of  $\chi(T)$ . The dependence  $\chi(T)$  is reasonably fitted by the following exponential function [39]:

$$\chi(T) = \chi_0 + \chi_1 \times \exp\left(\frac{\varepsilon}{kT}\right) \quad (6)$$

where  $\chi_0 = -0.52$  eV/atom,  $\chi_1 = 0.18$  eV/atom and  $\varepsilon = 0.11$  eV, respectively, for the considered  $\text{SiO}_{1.25}$  case. The analysis of  $\chi(T)$  for the other Si oxide compositions can be found in [39]. It should be noted that all the values of  $\chi(T)$  are comparable, and agree with the respective parameter value obtained in the framework of the phenomenological approach [37].

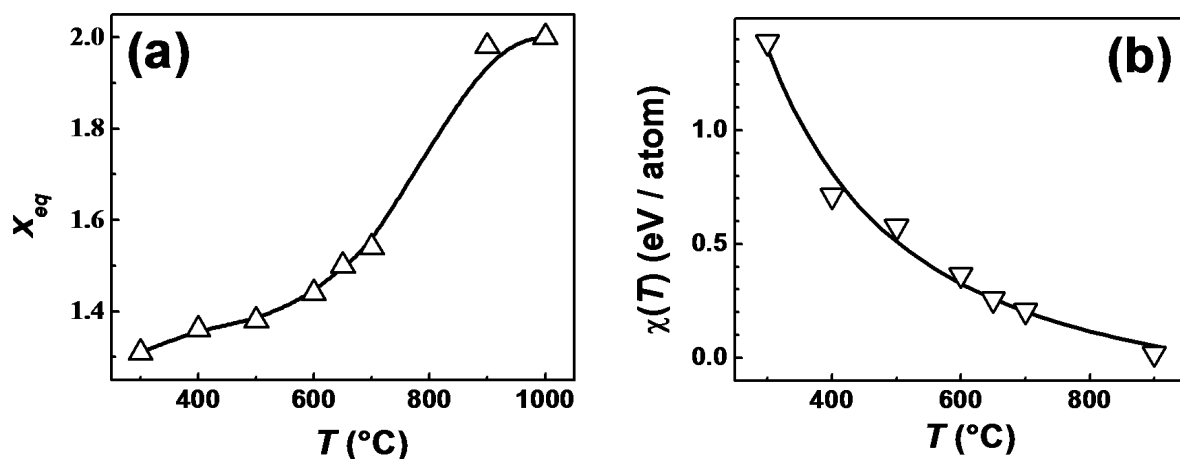


**Figure 5.** (a) The experimental temperature dependence of the equilibrium stoichiometry index of thermal vacuum sputtered  $\text{SiO}_{1.25}$  films [31] (symbols). The line is a guide for eyes. (b) The values of  $\chi(T)$  calculated using the data from panel (a) (symbols) and the approximation by the function (6) (line).

The dependences of  $g(x_0, x, T)$  on  $x$  calculated by the expressions (5) and (6), using the fitted parameters  $\chi_0$ ,  $\chi_1$ , and  $\varepsilon$ , are presented in Figure 6a,b for different initial  $\text{SiO}_x$  compositions and temperatures, respectively. The respective dependences of  $x_{eq}$  on the initial Si oxide stoichiometry and annealing temperature are shown in Figure 6c,d, respectively. As may be seen from this figure, the stress contribution to the Gibbs free energy of nano-Si/Si oxide systems enables us to reproduce the experimentally observed behavior of the equilibrium stoichiometry index of the Si oxide phase, with both its initial stoichiometry, and annealing temperature. The decrease in  $\chi(T)$  with temperature points to the temperature-induced stress relaxation in phase-separated systems. The parameter  $\varepsilon$  characterizes the activation energy of such relaxation. As can be further seen from Figure 5b, the internal stress is fully relaxed ( $\chi(T) = 0$ ) at temperatures above approximately 900 °C, which corresponds to complete  $\text{SiO}_x$  separation, and the formation of nearly stoichiometric

SiO<sub>2</sub> matrix composition. The appearance of internal stress has the most significant counteracting effect on the phase separation process. Therefore, together with the transformation of the penalty energy of Si-O<sub>y</sub>Si<sub>4-y</sub> tetrahedral units, as described in Section 2.1, this must be regarded as the main mechanism that defines the formation of equilibrium states in nano-Si/Si oxide systems.

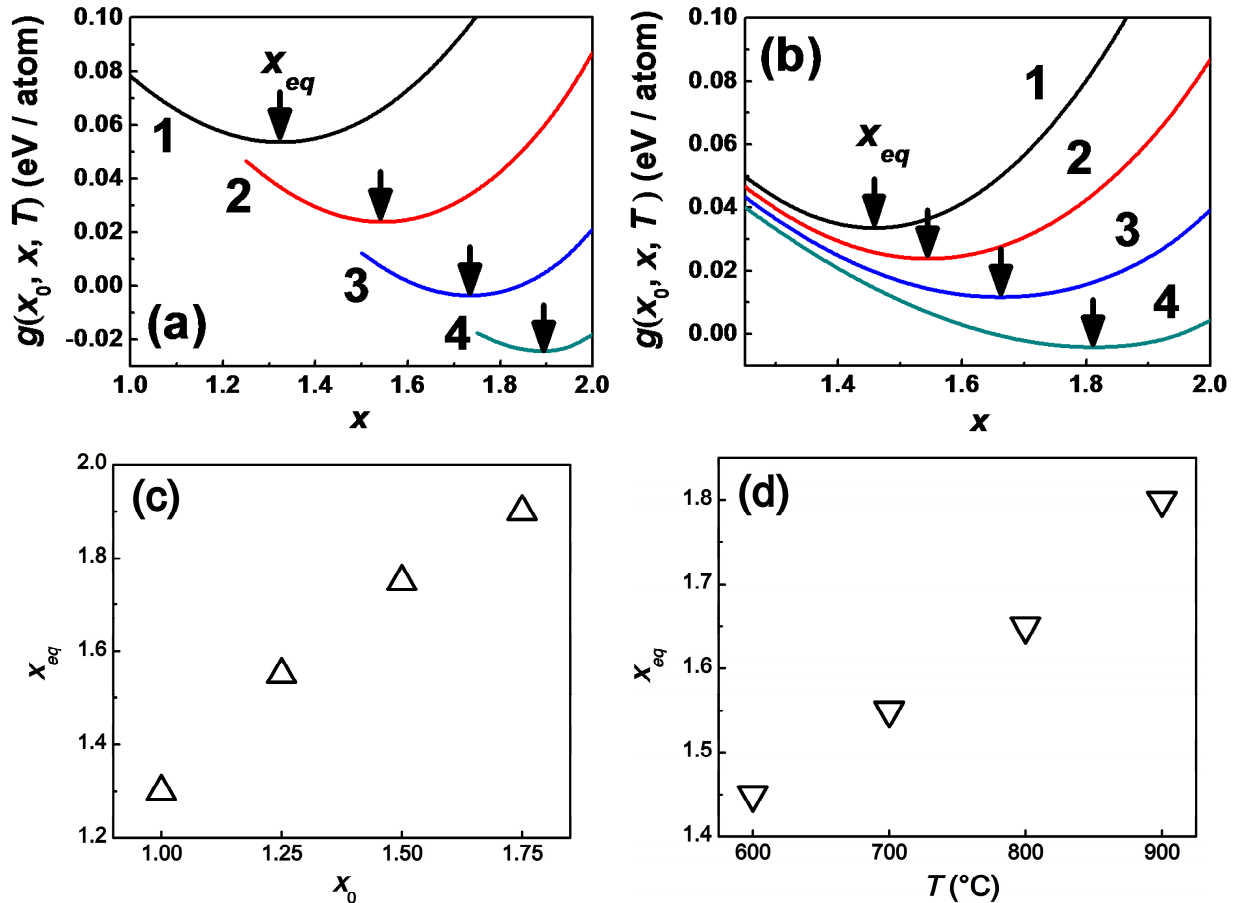


**Figure 6.** The dependence of the Gibbs free energy per one atom on the stoichiometry index of Si oxide in the a-Si/Si oxide systems, calculated by the expressions (5) and (6). (a) For different initial Si oxide stoichiometry indexes,  $x_0$ : 1—1, 2—1.25, 3—1.5, and 4—1.75. The annealing temperature  $T = 700^\circ\text{C}$ . (b) For different annealing temperatures,  $T$ : 1—600, 2—700, 3—800, and 4—900 °C. The initial Si oxide stoichiometry  $x_0 = 1.25$ . The arrows in the panels indicate the equilibrium stoichiometry indexes of the Si oxide phase. All the curves are shifted by  $\frac{1}{1+x_0} \frac{h_E - s_E T}{N_A}$  for better visualization. Panels (c) and (d) show the equilibrium stoichiometry index of Si oxide versus its initial stoichiometry and annealing temperature, recalculated using the data presented in panels (a) and (b), respectively.

#### 2.4. Crystallization Model of Amorphous Si Nanoinclusions Embedded in the Si Oxide Matrix

This section presents a crystallization model of Si nanoinclusions in Si oxide matrix formed as a result of SiO<sub>x</sub> phase separation [43]. The model considers the change in the Gibbs free energy of an a-Si particle with the radius  $R$  upon crystallization of its central part, as shown schematically in Figure 7. In this process, the Gibbs free energy decreases by  $\frac{4\pi r^3}{3\Omega} \Delta g_{ac}$  due to the crystallization of a sphere with the radius  $r$ , and increases by  $4\pi r^2(\gamma_{ac}^{eff} - \gamma_{oa}^{eff})$ , where  $\gamma_{oa}^{eff}$  and  $\gamma_{ac}^{eff}$  are the interface energies of the amorphous and crystalline Si spheres of radius  $r$ , inherently taking into account the interaction with the surrounding Si oxide matrix, according to the effective interface concept [43,64,65]:

$$\gamma_{oa}^{eff} = \gamma_{oa} \exp\left(-\frac{R-r}{l_0}\right), \quad \gamma_{ac}^{eff} = \gamma_{ac} + (\gamma_{oc} - \gamma_{ac}) \exp\left(-\frac{R-r}{l_0}\right) \quad (7)$$

Here,  $\gamma_{ac} = 0.231 \text{ J/m}^2$  [64],  $\gamma_{oc} = 0.41 \text{ J/m}^2$  [61], and  $\gamma_{oa} = \gamma_{oc} - 1.73 \times \gamma_{ac} = 0.01 \text{ J/m}^2$  [64] (see also Section 2.2) are the specific energies of a-Si/c-Si, c-Si/Si oxide, and a-Si/Si oxide interfaces, respectively, and  $l_0 = 2.532 \text{ \AA}$ , corresponding to the interatomic distance in crystalline Si, is regarded as the effective screening or bonding length related to the interatomic force range in Si and Si oxide materials [65].

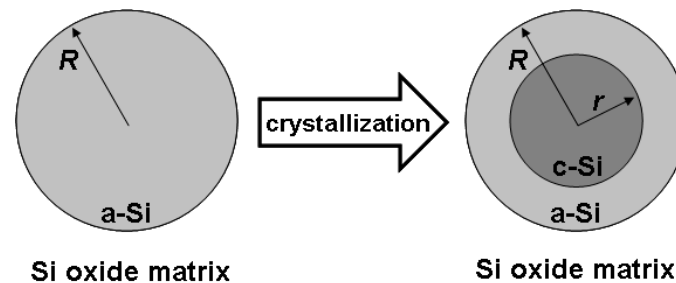


**Figure 7.** The geometry of amorphous (left) and partly crystallized (right) Si nanoinclusion in Si oxide matrix.

Hence, the crystallization of a central Si sphere with the radius  $r$  leads to the following change in the Gibbs free energy expressed per one atom in the initial a-Si nanoinclusion:

$$\Delta g_{cryst} = -\xi^3 \frac{h_E - s_E T}{N_A} + \frac{3\Omega\xi^2}{R} \left[ \gamma_{ac} + (\gamma_{oc} - \gamma_{ac} - \gamma_{oa}) \exp\left(-\frac{R(1-\xi)}{l_0}\right) \right] \quad (8)$$

where the relative radius of the internal crystallized part of the nanoinclusion  $\xi = \frac{r}{R}$  is introduced. The minimum values of the expression (8) define the equilibrium states of the Si nanoinclusion, while its maximum values set nucleation barriers for the amorphous-to-crystalline transition.

The calculations by the expression (8) enabled us to obtain the following main results concerning crystallization of a-Si nanoinclusions in Si oxide matrix, which are important for the further general analysis of the phase separation process in  $\text{SiO}_x$  films [43]:

1. The crystallization of an amorphous Si nanoinclusion is incomplete, and an amorphous shell between the crystalline core and the Si oxide matrix always remains. This result is illustrated by the exemplary dependences of  $\Delta g_{cryst}$  on  $\xi$ , for different initial radii  $R$  at  $900 \text{ }^\circ\text{C}$  presented in Figure 8a, in which  $\xi_{min}$  corresponds to the equilibrium states.
2. A minimum radius of amorphous Si nanoinclusions exists, below which crystallization becomes energetically unfavorable. The value of this radius increases with the increase in annealing temperature. The dependence of the Gibbs free energy change on  $\xi$  for a Si nanoinclusion, with the radius below the crystallization threshold, is illustrated by the curve (1) in Figure 8.
3. The crystallized Si fraction (value of  $\xi_{min}$ ) increases, and the nucleation barrier for crystallization decreases, with the increase in a-Si nanoinclusion size, due to the weakening of the influence of the Si oxide matrix on the crystallization process. The saturation of the nucleation barrier at  $R \approx 2 \text{ nm}$  points to an almost complete loss of this influence. This result is illustrated by the dependences presented in Figure 9a,b for the crystallization temperature of  $900 \text{ }^\circ\text{C}$  (see also Figure 8a,b).

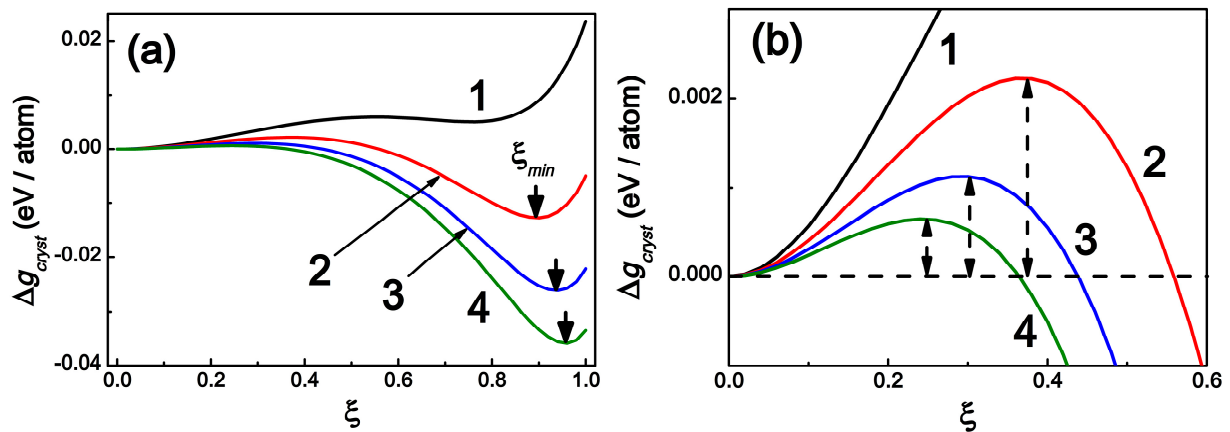


**Figure 8.** Dependence of the Gibbs free energy per atom of a spherical Si inclusion in the Si oxide matrix upon the relative radius of its internal crystallized part at  $T = 900$  °C for different Si radii  $R$ : 1—1.5, 2—2, 3—2.5, and 4—3 nm. The arrows in panel (a) indicate the equilibrium values of the relative radius of the internal crystallized part of the nanoinclusions. The double arrows in panel (b) show the nucleation barriers for crystallization.

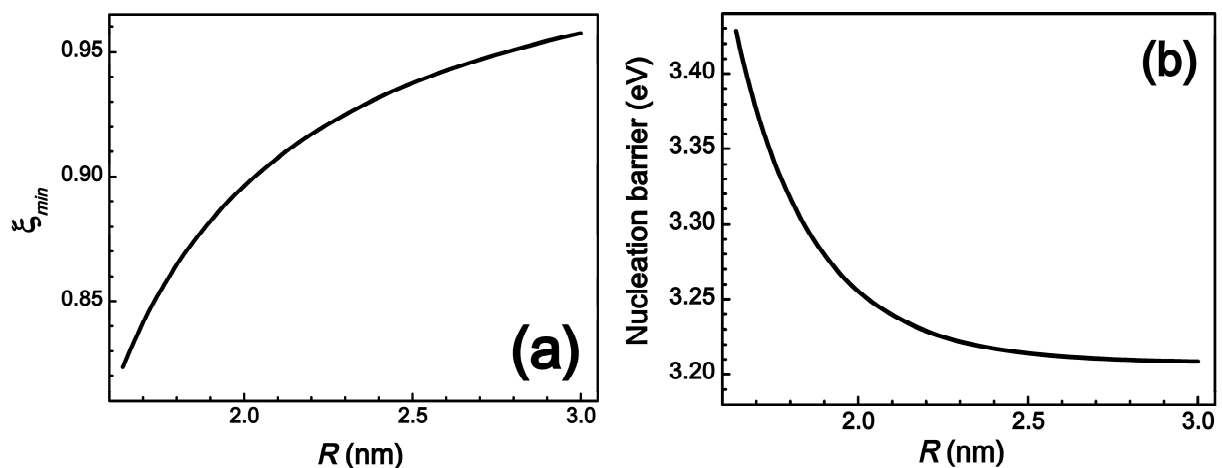


**Figure 9.** The dependence of the relative radius of the internal crystallized part corresponding to the minimum Gibbs free energy (a) and nucleation barrier (b), on the radius of the initially amorphous Si nanoinclusion in the Si oxide matrix at  $T = 900$  °C.

It should be noted, as well, that both the nucleation barrier increases, and  $\xi_{min}$  decreases, with temperature. This has an effect on the Si crystallization kinetics, and the distribution function of Si nanocrystals in the Si oxide matrix [43].

### 3. Discussion

In this section, a general analysis of the phase separation process, during the annealing of nonstoichiometric Si oxides, is provided. We discuss the elementary stages of this process, the mechanisms governing the system's evolution, and the dependence of the characteristics of formed nano-Si/Si oxide composites on the initial Si oxide parameters and annealing temperature.

As was already mentioned in Section 2.1, all the mechanisms that act during the phase separation of  $\text{SiO}_x$  films are characterized by their contributions to the Gibbs free energy of Si/Si oxide systems [38,41,42]. Here, the role of a particular mechanism on promoting or counteracting phase separation is determined by whether the corresponding Gibbs free energy contribution decreases or increases with the increase in  $x$ .

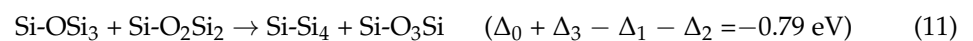
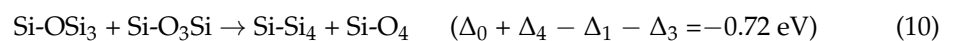
As demonstrated in both experimental and theoretical investigations, the phase separation in nonstoichiometric Si oxides is consistent with the redistribution of oxygen atoms from the oxygen poor to the oxygen rich Si–O<sub>y</sub>Si<sub>4–y</sub> tetrahedral units that compose the SiO<sub>x</sub> microstructure [31,66–68]. In particular, it was shown [31] that too low values of Si diffusivity in Si oxide do not allow the description of the experimental very fast kinetics of SiO<sub>x</sub> separation (~ 1 s at 1000 °C) using the mechanism of Si diffusion and agglomeration. On the other hand, IR absorption studies revealed [66] that during the annealing of SiO<sub>x</sub>, weakly oxidized Si–O<sub>y</sub>Si<sub>4–y</sub> units (basically Si–OSi<sub>3</sub>) become Si–Si<sub>4</sub> by losing oxygen atoms, which are captured by strongly oxidized complexes, such as Si–O<sub>3</sub>Si. Oxygen in various configurations is a fast diffuser in Si oxide, and its diffusivity agrees with the experimental phase separation kinetics [31]. It was hypothesized, therefore [66], that the oxygen release at the nano-Si/Si oxide interfaces, and its diffusion into the matrix bulk, should define the phase separation of SiO<sub>x</sub> films, and the consistency of this hypothesis was confirmed by kinetic simulations [67,68].

The character of the composition change in Si oxide by oxygen redistribution between the Si–O<sub>y</sub>Si<sub>4–y</sub> tetrahedral units may be easily understood, by referring to the unit penalty energies Δ<sub>y</sub> (see Section 2.1). Namely, the transition of an oxygen atom between two Si–O<sub>y</sub>Si<sub>4–y</sub> units reduces their total penalty energy, only if the difference between their oxidation degrees (values of *y*) increases. Therefore, the transformation of an initially homogeneous nonstoichiometric Si oxide into a composite, consisting of separated Si and SiO<sub>x</sub> phases, is caused by the tendency to minimize the penalty energy of the entire Si/Si oxide system as the principal mechanism. A complete separation into the stoichiometric Si and SiO<sub>2</sub> would reduce the total penalty energy to zero. Considering this mechanism alone, van Harpert et al. [69] concluded that the equilibrium state in Si/Si oxide systems corresponds to the coexistence of the Si and SiO<sub>2</sub> phases, as providing zero total penalty energy of all the Si–O<sub>y</sub>Si<sub>4–y</sub> tetrahedral units.

Moreover, taking into account the values of Δ<sub>y</sub>, we may also be able to explain the evolution of an initial Si oxide by the separation of purely Si nano-inclusions in the Si oxide matrix, with a gradually increasing stoichiometry index instead of the formation of two Si oxide phases, the one with a gradually decreasing, and the other with a gradually increasing, stoichiometry index. Indeed, imagine the transition of an oxygen atom between two Si–O<sub>2</sub>Si<sub>2</sub> units, according to the following reaction:



As a result, the Gibbs free energy changes by Δ<sub>1</sub> + Δ<sub>3</sub> – 2Δ<sub>2</sub> = –0.3 eV. The reaction products may further evolve, according to the following reactions:



where the change in the Gibbs free energy in each reaction is provided in parenthesis.

The reactions (10)–(12) show that when a Si–O<sub>2</sub>Si<sub>2</sub> tetrahedral unit loses an oxygen atom, it is energetically favorable to lose the remaining oxygen atom, converting to the Si–Si<sub>4</sub> unit of a pure Si phase. Hence, the local separation of pure Si in the form of nanoparticles takes place. On the other hand, when a Si–O<sub>2</sub>Si<sub>2</sub> unit acquires an oxygen atom, the next atom would be taken by another unit of the same composition, rather than by the freshly formed Si–O<sub>3</sub>Si one. Therefore, no local inclusions of the SiO<sub>2</sub> composition form, and the stoichiometry index of the Si oxide matrix evolves homogeneously. The processes described by the reactions (10)–(12), together with the respective energy changes, are schematically depicted in Figure 10.

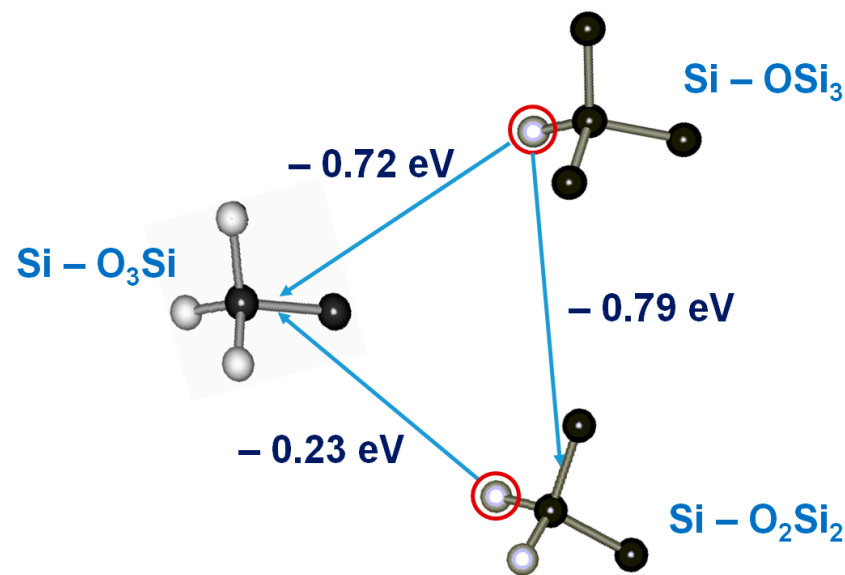


**Figure 10.** A schematic representation of the processes, according to the reactions (10)–(12), with respective changes in the penalty energy of the participating  $\text{Si-O}_y\text{Si}_{4-y}$  tetrahedral units. The Si atoms are shown in black, and white corresponds to oxygen atoms.

The separation of Si and Si oxide (the increase in the value of  $x$ ) also leads to a decrease in the configuration entropy, due to the reduction in the number of arrangements of oxygen atoms between the pairs of Si atoms in the Si oxide phase. The entropy decrease results in the growth in the respective contribution to the Gibbs free energy. Another Gibbs free energy term increasing with  $x$  is related to the separation of the amorphous Si phase (see expression (2)). Therefore, both mechanisms counteract the phase separation of nonstoichiometric Si oxides. At this, the changes in the corresponding terms with  $x$  are noticeably smaller, compared to the total penalty energy change (for example, the absolute value of the change in the total penalty energy upon transformation of an initial  $\text{SiO}_{1.0}$  into the  $\text{Si/SiO}_{1.9}$  system at  $900\text{ }^\circ\text{C}$  is equal to about  $0.17\text{ eV/atom}$ , while the entropy and amorphous Si related contributions change at this by about  $0.06$  and  $0.02\text{ eV/atom}$ , respectively). Therefore, the role of the former mechanisms on the formation of the equilibrium states in Si/Si oxide systems is substantially weaker than that of the latter mechanism. The configuration entropy contribution alone defines the temperature dependence of the excess Si concentration (solubility limit) in  $\text{SiO}_2$  in equilibrium with crystalline Si, while, together with the a-Si related term, it defines the solubility of a-Si in  $\text{SiO}_2$ , which is noticeably higher than that of c-Si [38].

It should also be mentioned that the formation of interfaces between the nano-Si inclusions and the Si oxide matrix introduces a contribution to the Gibbs free energy, three to four orders of magnitude smaller than the penalty-energy-related term (see Section 2.2). Therefore, although this process counteracts phase separation, it plays a minor role on equilibrium states in nano-Si/Si oxide systems, and may not be considered.

As demonstrated in Section 2.3, the appearance of internal stress is the key mechanism that causes an incomplete separation into the Si and  $\text{SiO}_x$  phases, and a remarkable dependence of the equilibrium Si oxide stoichiometry on the annealing temperature. We have to note that up to now, we have not been able to propose a unique unambiguous model of stress formation in phase separated Si/Si oxide systems. The main problem we encounter is that each developed model contains a number of fitting parameters no less than the semi-empirical description presented in Section 2.3. This leaves the question about the correctness of a particular model open, and at the same time offers no advantages in calculating the stress-related Gibbs free energy contribution, compared to using the function  $\chi(T)$ .

The mechanisms of stress formation during the phase separation of nonstoichiometric Si oxides may be discussed as follows. Let us consider oxygen out-migration from the regions where nano-Si inclusions form, into the surrounding Si oxide matrix, as illustrated schematically in Figure 11 for a single nanoinclusion case. Si atoms, which will constitute the Si nanoparticle, are located in a certain volume 2 of the initial Si oxide, as indicated in the left-hand side of Figure 11. As oxygen atoms leave this volume, the latter may shrink, as shown in the right-hand side of Figure 11, ideally down to the volume 4 of a fully relaxed Si phase. If, however, no complete Si relaxation occurs, and the volume 3 of the separated Si phase remains in excess to that of the relaxed Si, tensile stress is exerted on the Si nanoparticle. In turn, the redistributed oxygen atoms incoming into the Si oxide matrix around the formed nanoinclusion increase the total atomic concentration within it, leading to the appearance of compressive strain and corresponding stress, if only partial matrix relaxation is achieved.

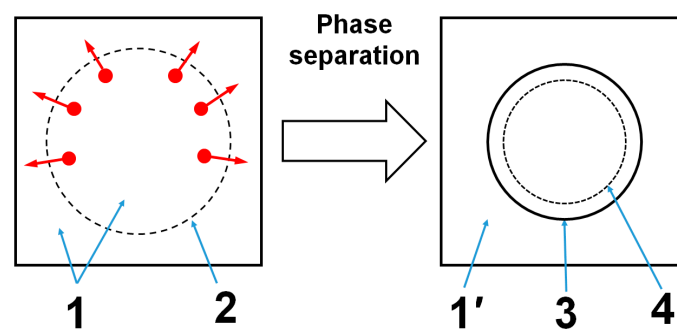


**Figure 11.** The formation of amorphous Si nanoinclusion by the out-migration of oxygen, during the phase separation of nonstoichiometric Si oxide. Left part: (1) the initial Si oxide phase, (2) the boundary of the volume from which oxygen out-migration takes place. Red disks schematically represent oxygen atoms, while red arrows indicate the directions of their redistribution. Right part: (1') the Si oxide phase with increased stoichiometry index, compared to the initial one, (3) the boundary of the formed Si nanoinclusion with exerted tensile stress, (4) the boundary of the fully relaxed Si nanoinclusion.

The simplest model of stress formation during phase separation in  $\text{SiO}_x$  films [40] assumes that the volume of the Si oxide phase does not change with new incoming oxygen atoms, and also that the Si phase is fully relaxed (region 4 in Figure 11). Therefore, only the compressive stress in the Si oxide matrix is considered. According to Hook's law, the stress-related energy per unit volume is calculated as follows:

$$G_{stress} = \frac{1}{2} K_{\text{SiO}_x} \left( \frac{\Delta V}{V_x} \right)^2 = \frac{1}{2} K_{\text{SiO}_x} \left( \frac{V_x - V_{x0}}{V_x} \right)^2 \quad (13)$$

where  $V_x$  is the volume that the  $\text{SiO}_x$  phase with the stoichiometry index  $x$  would have in a relaxed state;  $V_{x0}$  is the actual volume of the Si oxide phase corresponding to the initial stoichiometry index  $x_0$ ; and  $K_{\text{SiO}_x} = 2.53 \times 10^{10}$  Pa is the bulk modulus of the Si oxide phase [70], assumed not to depend on the stoichiometry index  $x$ , respectively.

The dependence of the  $\text{SiO}_x$  volume on its stoichiometry may be written using the composition expansion of Si oxide with a constant number of Si atoms  $\eta = \frac{1}{V_0} \frac{\partial V_x}{\partial x}$  as follows:

$$V_x = V_0(1 + \eta x) \quad (14)$$

Here,  $\eta = \frac{V_{\text{SiO}_2} - V_{\text{Si}}}{2V_{\text{Si}}} \approx 0.6$  is calculated, taking into account that the volume of Si oxide at  $x = 2$  corresponds to the volume of the stoichiometric  $\text{SiO}_2$  phase,  $V_{\text{SiO}_2}$ , while at  $x = 0$ , it is the volume of the Si phase,  $V_{\text{Si}}$ , respectively, as well as  $\frac{V_{\text{SiO}_2}}{V_{\text{Si}}} \approx 2.2$  as follows from the experimentally observed swelling of the Si volume by about 2.2 times, after the thermal oxidation of the Si wafers [71].

Therefore, the stress-related energy per unit volume of the Si oxide phase takes the following form:

$$G_{stress} = \frac{1}{2} K_{SiO_x} \eta^2 \frac{(x - x_0)^2}{(1 + \eta x)^2} \quad (15)$$

For  $\eta x \ll 1$ , the expression (15) is fully equivalent to the stress-related Gibbs free energy per unit volume introduced in [37], except that there, a linear, not a bulk, deformation was considered.

In the proposed description of the stress origin, the function  $\frac{K_{SiO_x} \eta^2}{2(1 + \eta x)^2}$  in the expression (15) must be equivalent to the function  $\chi(T)$  in the expression (5). The temperature dependence of the former function is caused by the respective temperature dependence of  $\eta$  or, more particularly, of the volumes  $V_{SiO_2}$  and  $V_{Si}$ . The calculations [40] show, however, that the temperature dependence of the function in the expression (15) is negligible, compared to that of  $\chi(T)$  obtained in Section 2.3, and does not allow us to explain the experimentally observed variations of  $x_{eq}$  with the annealing temperature. This means that the stress decreases with temperature, not only due to the different values of the thermal expansion coefficients of Si and SiO<sub>2</sub>, but also due to the action of additional mechanisms of stress relaxation.

Further developments in the presented model include accounting for other possible stress contributions, such as the hydrostatic tensile stress in Si nanoparticles, when the nano-Si volume 3 remains larger than the volume 4, corresponding to the fully relaxed case (see Figure 11), and the stress related to maintaining coherency at the Si/Si oxide interfaces. Each iteration of the model complicates its expressions, and introduces new fitting parameters that take into account, for example, the different degrees of Si and SiO<sub>x</sub> relaxation, the redistribution of strain between the Si and SiO<sub>x</sub> phases caused by a large difference in their elastic modules [72], the degree of incoherency at the Si/Si oxide interfaces, etc., which makes the calculation of the strain-related Gibbs free energy completely inefficient. It is advised, therefore, to keep in mind a basic understanding of the mechanism of the stress origin during the phase separation in nonstoichiometric Si oxides, to use the semi-empirical expression  $\Delta g_{stress} = \chi(T)(x - x_0)^2$ , which requires to fit only three parameters of the function  $\chi(T)$ .

The descending character of  $\chi(T)$  points to the enhancement of stress relaxation when the annealing temperature is increased. As may be seen from Figure 5,  $\chi(T) = 0$  at about 900 °C, which constitutes complete stress relaxation and separation into Si and close-to-stoichiometric SiO<sub>2</sub> phases. This finding correlates with the results obtained by Lukovsky et al. [73], who investigated the behavior of SiO<sub>x</sub>/SiO<sub>2</sub> interfaces during growth of SiO<sub>2</sub> on crystalline Si layers. It was found that a nonstoichiometric transition layer underwent separation at the temperature of about 900 °C, due to bond switching, which led to the transformation of the initially stressed transition layer into the relaxed one. This process was accompanied by an increase in the SiO<sub>2</sub> layer thickness. Therefore, stress relaxation in phase-separating Si oxides may be considered by bond switching at the Si/Si oxide interfaces, and in the Si oxide bulk. The probability of bond switching increases with temperature, as a certain energy barrier must be overcome. The same temperature of complete relaxation of nonstoichiometric Si oxide observed by Lukovsky et al. [73], and for achieving zero value of  $\chi(T)$ , strongly supports the bond-switching mechanism of stress relaxation during phase separation in SiO<sub>x</sub> films.

The annealing of nonstoichiometric Si oxide films first leads to the separation of amorphous Si nanoinclusions. These nanoinclusions may then partially or almost fully crystallize, or remain amorphous, depending on their size and annealing temperature. The experimental results [28] supported by the theoretical calculations [43] demonstrate that the crystalline Si fraction in Si/Si oxide composites increases with the annealing temperature of SiO<sub>x</sub> films. According to our crystallization model, outlined in Section 2.4, this increase is related to the growth in the nano-Si radii due to the increase in the amount of separated Si or the coalescence of Si nanoparticles at the temperatures above 1000 °C [28] (the relative

radius of the crystallized Si part  $\xi_{min}$  increases, and the nucleation barrier decreases, with the increase in  $R$ , see Figure 9).

The phenomenon not addressed so far is the influence of the partial crystallization of Si nanoinclusions on equilibrium in Si/Si oxide systems. The Gibbs free energy of c-Si is smaller, compared to that of a-Si (see Section 2.1). Therefore, crystallization of a part of the Si nanoparticle must lead to additional Si separation from the surrounding Si oxide matrix, resulting in the increase in nano-Si radius. In its turn, the increase in the nanoparticle radius promotes a further increase in  $\xi_{min}$ , and so forth. It may be concluded, therefore, that the crystallization process is expected to induce significant transformations of both the nanoinclusion size and crystalline state, as well as the stoichiometry of the surrounding Si oxide matrix.

Figure 12 shows the transformation of an exemplary a-Si nanoinclusion with a radius of 2 nm, embedded in a  $\text{SiO}_{1.8}$  matrix obtained as a result of the phase separation of a  $\text{SiO}_{1.25}$  film at 900 °C. The values of the initial and final stoichiometry indexes of the Si oxide, corresponding to the chosen temperature, are taken with reference to Figure 6b,d. The search for the minimum values of the Gibbs free energy obtained by combining the expressions (2) and (8) demonstrates that the nanoinclusion radius increases to about 2.13 nm in the equilibrium state. The relative radius of the crystallized part becomes  $\xi_{min} = 0.91$ , which is somewhat larger than the respective value  $\sim 0.89$  for the crystallization of the initial a-Si nanoinclusion. The increase in the radius occurs by the separation of additional Si from the surrounding matrix. The matrix stoichiometry becomes about 1.98, which is close to that of the stoichiometric  $\text{SiO}_2$ , and corresponds to the equilibrium between the Si oxide and the crystalline Si phase at 900 °C. The same effect was always reproduced in multiple calculations for different a-Si radii, as well as different initial and final  $\text{SiO}_x$  stoichiometries. The obtained result naturally explains an experimentally observed correlation between the appearance of the  $\text{SiO}_2$ -related peaks in the IR absorption spectra, and the characteristic photoluminescence (PL) band of Si nanocrystals [34], implying that the crystalline Si phase and  $\text{SiO}_2$  regions are always formed together during the phase separation of nonstoichiometric Si oxide films.

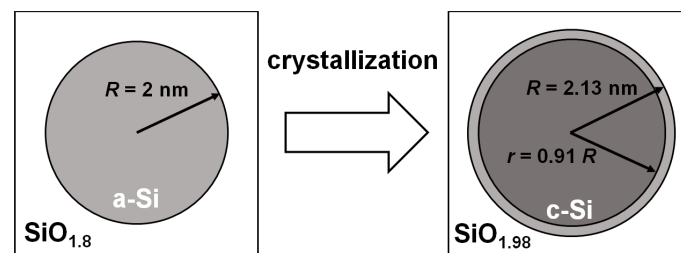


**Figure 12.** The transformation of a-Si nanoinclusion with a radius  $R = 2$  nm, embedded in a  $\text{SiO}_{1.8}$  matrix as a result of the crystallization of its internal part.

We may now use the general thermodynamic theory to discuss the peculiarities of the formation of Si/Si oxide composites by the phase separation of nonstoichiometric Si oxides as functions of the annealing temperature. Here, we will also refer to the results of experimental investigations of the temperature dependence of the characteristics of phase separated Si/Si oxide systems obtained by IR absorption spectroscopy, XPS, Raman scattering, and photoluminescence investigations [32–34,74–76].

The experimental studies report the beginning of the phase separation process at temperatures between approximately 300 and 600 °C, depending on the technology of the initial Si oxide fabrication and annealing conditions [32,33,75]. The raise of the annealing temperature leads to the increase in the amount of separated Si, which is manifested by the increase in the stoichiometry index of the Si oxide matrix, revealed by IR spectroscopy, as well as by the growth in the intensity of the  $\text{Si}^0$  band in the XPS spectra [33,34,75], and the shift of the PL peak position toward longer wavelengths [32,34,74]. The increase in the degree of phase separation with the annealing temperature corresponds to the temperature-

enhanced stress relaxation in Si oxide films, as shown in Section 2.3, and discussed earlier in this section. Purely amorphous Si nanoinclusions form at annealing temperatures up to 800 °C, as inferred by observations in the Raman spectra of the characteristic broad band, peaked at  $\sim 480 \text{ cm}^{-1}$ , corresponding to the amorphous Si phase [32,76]. The Si oxide matrix of Si/Si oxide composites formed at such temperatures is essentially nonstoichiometric, without SiO<sub>2</sub> inclusions, as demonstrated by the presence of only the characteristic for the SiO<sub>x</sub> ( $x < 2$ ) elementary bands in the respective IR absorption spectra [34]. The formation of purely amorphous Si inclusions is explained by their small sizes below the crystallization threshold, as described in Section 2.4.

Raising the annealing temperature above 800 °C induces the onset of Si particle crystallization, as demonstrated in particular by the appearance in the Raman spectra of annealed films of the narrow peak at  $\sim 519 \text{ cm}^{-1}$ , corresponding to the crystalline Si phase [33,76]. According to the thermodynamic theory presented in this paper, Si nanoinclusions crystallize when their sizes reach the minimum crystallization size at a given temperature. By accepting the average density of Si nanoinclusions  $C_{incl} = 10^{19} \text{ cm}^{-3}$ , the initial stoichiometry index of SiO<sub>x</sub>  $x_0 = 1.25$  and the equilibrium stoichiometry index at 800 °C  $x_{eq} = 1.7$  (see Figure 5a), the average radius of separated Si nanoparticles of  $\sim 1.65 \text{ nm}$  is obtained. At the same time, the crystallization model presented in Section 2.4 provides the minimum crystallization radius at this temperature to be  $\sim 1.6 \text{ nm}$ . Repeating the same calculations for 700 °C, one obtains the average nanoparticle radius and the minimum crystallization radius of  $\sim 1.4$  and more than  $1.5 \text{ nm}$ , respectively. Therefore, the temperature of crystallization starting close to 800 °C is theoretically justified.

In view of the distribution function of Si nanoinclusions on size, their crystallization does not take place at a single temperature value. The crystallization degree increases with the increase in the annealing temperature, up to about 1150 °C, when complete crystallization is obtained. Both amorphous and crystalline Si-related bands are observed in the Raman and photoluminescence spectra of SiO<sub>x</sub> samples annealed below this temperature [32–34,76]. Along with this, the IR absorption spectra are composed by the elementary bands corresponding to Si–O<sub>y</sub>Si<sub>4–y</sub> tetrahedral complexes in the nonstoichiometric Si oxide phase, as well as Si–O<sub>4</sub> tetrahedra in 4- and 6-member rings of the SiO<sub>2</sub> phase [34]. Hence, Si/Si oxide composites obtained at the temperatures between approximately 800 and 1150 °C contain larger crystalline and smaller amorphous Si nanoinclusions, surrounded respectively by the nonstoichiometric SiO<sub>x</sub>, and the nearly stoichiometric SiO<sub>2</sub> phase, formed as a result of Si crystallization, as described earlier in this section.

At higher annealing temperatures, the efficient coalescence of Si nanoparticles is observed, leading to the increase in their average size [28,30]. At such temperatures, the portion of the amorphous Si phase is small, and the signals from the Si nanocrystallites dominate in the Raman and PL spectra of annealed SiO<sub>x</sub> films [32–34]. From a thermodynamic point of view, the major part of Si nanoparticles becomes larger than the crystallization threshold, due to coalescence, and therefore convert into Si nanocrystals. The amorphous Si-related contributions to the Raman spectra may come from the tail of the size distribution function of Si nanoparticles, and/or amorphous Si shells linking the Si nanocrystals to the surrounding Si oxide matrix.

Our theory may now be compared to the only other known thermodynamic approach to studying phase separation in nonstoichiometric Si oxide films [37]. This approach uses the phenomenological expression for the density of the Gibbs free energy of nonstoichiometric Si oxides in the following form:

$$\tilde{g}_{SiO_x}(x, x_0, T) = -\alpha(T)(x - 1)^2 + \beta(T)(x - 1)^4 + \frac{1}{2}E[\varepsilon_0(x - x_0)]^2 \quad (16)$$

where the functions  $\alpha(T)$  and  $\beta(T)$  are chosen based on the work of Schnurre et al. [36], to ensure the stability of the Si and SiO<sub>2</sub> phases, as well as the metastability of the SiO phase;  $E$  is the Young's modulus of Si oxide,  $\varepsilon_0 = \frac{1}{a} \frac{\partial a}{\partial x}$  is the composition expansion coefficient of Si oxide, and  $a$  is the average atomic distance in the Si oxide, respectively.

As demonstrated in [37], the theory based on the expression (16) predicts qualitatively similar behavior in the characteristics of the nonstoichiometric Si oxides, as a function of the initial  $\text{SiO}_x$  composition and annealing temperature. However, such a theory is oversimplified, as it does not consider, for example, the free energy contribution of the separated Si phase, the microstructure of Si oxide composed of  $\text{Si-O}_y\text{Si}_{4-y}$  units with different energy characteristics, the entropy transformation during phase separation, the possible crystallization of Si nanoparticles, and a number of other important aspects. Moreover, it does not provide a good quantitative agreement with the experimental data. Conversely, the thermodynamic theory developed in the present paper is comprehensive, and adequately describes all the characteristic features of the phase separation process in nonstoichiometric Si oxide films, as functions of the annealing temperature and the initial  $\text{SiO}_x$  composition.

#### 4. Conclusions

In this paper, a thermodynamic theory of phase separation in nonstoichiometric Si oxide films ( $\text{SiO}_x$ ,  $x < 2$ ) during high-temperature anneals is developed. The theory is based on a number of thermodynamic models, addressing various aspects of the phase separation process reported in our previous publications. A brief review of these models was presented, as required in order to understand the studied process in its integrity.

The expression for the Gibbs free energy of Si oxides and amorphous (crystalline) Si/Si oxide systems is derived. The analysis of the transformations of the Gibbs free energy, with the change in the Si oxide composition during the phase separation process, as the function of the initial Si oxide stoichiometry and the annealing temperature, has enabled us to clarify the roles of different mechanisms in the formation of equilibrium states in nano-Si/Si oxide systems. It has been found that the driving force of  $\text{SiO}_x$  decomposition is the tendency toward the minimization of the total penalty energy of the  $\text{Si-O}_y\text{Si}_{4-y}$  tetrahedral units composing the Si oxide microstructure. The specific values of the penalty energy of the  $\text{Si-O}_y\text{Si}_{4-y}$  units with a different  $y$  cause the localized separation of the pure Si phase, as well as the homogeneous increase in the stoichiometry index of the Si oxide matrix, which is a characteristic feature of the phase decomposition in nonstoichiometric Si oxide films.

The formation of internal stress during Si and Si oxide separation is found to be the key mechanism that counteracts this process, and defines the equilibrium states in separated nano-Si/Si oxide systems (the amount of separated Si, and the stoichiometry index of the  $\text{SiO}_x$  matrix), as functions of the initial Si oxide composition and the annealing temperature. The mechanisms of stress formation in the process under study are discussed. It is demonstrated that the stress value decreases with the annealing temperature, presumably by bond switching at the nano-Si/Si oxide interfaces, and in the  $\text{SiO}_x$  bulk.

The crystallization of separated amorphous Si nanoinclusions in the Si oxide matrix is modeled. The equilibrium state of a Si nanoinclusion corresponds to incomplete crystallization in all cases, with an amorphous Si layer remaining at the crystalline Si core/Si oxide matrix interface. The relative radius of the crystallized Si part increases, and the nucleation barrier for crystallization decreases, with the increase in the Si nanoinclusion radius. It is demonstrated that the partial crystallization of an a-Si nanoparticle induces additional separation of Si from the surrounding Si oxide matrix, leading to the increase in the nanoparticle size. In its turn, this causes the relative size of the crystallized Si core to grow, etc. This process continues, until equilibrium between almost fully crystallized Si nanoinclusion, surrounded by the Si oxide matrix with the stoichiometry index  $x \approx 2$ , is established. This result enables us to explain the experimentally observed correlation of the presence of a-Si inclusions with the nonstoichiometric  $\text{SiO}_x$  phase, as well as c-Si inclusions with the  $\text{SiO}_2$  phase in the Si oxide matrix of the phase-separated nano-Si/Si oxide systems.

The characteristic features of the phase separation process as the functions of annealing temperature are discussed within the framework of the general thermodynamic theory developed in this paper. At lower temperatures (600–800 °C), amorphous Si nanoinclusions, with sizes below the crystallization threshold, are formed in the non-stoichiometric Si oxide

matrix. At temperatures between approximately 800 and 1150 °C, the crystallization of Si nanoinclusions, with sizes larger than the crystallization critical size, takes place. The Si crystallization induces additional separation of Si from the Si oxide matrix, and the formation of the regions of the nearly stoichiometric SiO<sub>2</sub> phase within it. Finally, high annealing temperatures (above ~1150 °C) promote the coalescence of Si nanoinclusions, and their efficient crystallization, due to large sizes. The amorphous Si phase is present in the smallest nanoinclusions, and at the Si nanocrystals/Si oxide matrix interfaces.

As demonstrated in Figure 1, the thermodynamic models composing the general theory were successfully applied in the studies, beyond the thermodynamics of phase separation in SiO<sub>x</sub> films. In particular, the analysis of the composition dependence of the Gibbs free energy of Si oxide enabled us to obtain its binodal and spinodal characteristics, and determine the stoichiometry ranges corresponding to the stability of the Si oxide phase, and phase separation, according to the nucleation and growth, and spinodal decomposition mechanisms [44]. The application of the Gibbs free energy (2) to SiO<sub>x</sub>(N<sub>y</sub>)/SiO<sub>2</sub> superlattices with nanometer thick layers made it possible to find the mechanism of layer intermixing within them, and to determine the critical layer thicknesses for intermixing as the functions of annealing temperature [47–49]. Finally, it was demonstrated, by comparing the Gibbs free energies of different Si oxynitride structures, that low stoichiometries and deposition temperatures (~300–400 °C) promote the formation of two-phase (oxide- and nitride-like) structures consistent with the random mixture model description. On the other hand, homogeneous films corresponding to the random bonding model are formed at increased stoichiometry indices and high deposition temperatures (~800–900 °C).

**Funding:** This research received no external funding.

**Data Availability Statement:** The data presented in this study may be provided by the author upon reasonable request.

**Conflicts of Interest:** The author declares no conflict of interest.

## References

1. Irrera, A.; Franzò, G.; Iacona, F.; Canino, A.; Di Stefano, G.; Sanfilippo, D.; Piana, A.; Fallica, P.D.; Priolo, F. Light emitting devices based on silicon nanostructures. *Physica E* **2007**, *38*, 181. [\[CrossRef\]](#)
2. Wang, M.; Anopchenko, A.; Marconi, A.; Moser, E.; Prezioso, S.; Pavese, L.; Pucker, G.; Bellutti, P.; Vanzetti, L. Light emitting devices based on nanocrystalline-silicon multilayer structure. *Physica E* **2009**, *41*, 912. [\[CrossRef\]](#)
3. Tsoukalas, D.; Dimitrakis, P.; Kolliopoulou, S.; Normand, P. Recent advances in nanoparticle memories. *Mater. Sci. Eng. B* **2005**, *124–125*, 93. [\[CrossRef\]](#)
4. Bratus', O.L.; Evtukh, A.A.; Ievtukh, V.A.; Litovchenko, V.G. Nanocomposite SiO<sub>2</sub>(Si) films as a medium for non-volatile memory. *J. Non-Cryst. Solids* **2008**, *354*, 4278. [\[CrossRef\]](#)
5. Shieh, J.-M.; Lai, Y.-F.; Ni, W.-X.; Kuo, H.-C.; Fang, C.-Y.; Huang, J.Y.; Pan, C.-L. Enhanced photoresponse of a metal-oxide-semiconductor photodetector with silicon nanocrystals embedded in the oxide layer. *Appl. Phys. Lett.* **2007**, *90*, 051105. [\[CrossRef\]](#)
6. Yu, Z.; Aceves-Mijares, M. A ultraviolet-visible-near infrared photodetector using nanocrystalline Si superlattice. *Appl. Phys. Lett.* **2009**, *95*, 081101. [\[CrossRef\]](#)
7. Evtukh, A.A.; Litovchenko, V.G.; Semenenko, M.O. Electrical and emission properties of nanocomposite SiO<sub>x</sub>(Si) and SiO<sub>2</sub>(Si) films. *J. Vac. Sci. Technol. B* **2006**, *24*, 945. [\[CrossRef\]](#)
8. Semenenko, M.; Evtukh, A.; Yilmazoglu, O.; Hartnagel, H.L.; Pavlidis, D. A novel method to form conducting channels in SiO<sub>x</sub>(Si) films for field emission application. *J. Appl. Phys.* **2010**, *107*, 013702. [\[CrossRef\]](#)
9. Yan, B.; Yue, G.; Sivec, L.; Yang, J.; Guha, S.; Jiang, C.-S. Innovative dual function nc-SiO<sub>x</sub>:H layer leading to a >16% efficient multi-junction thin-film silicon solar cell. *Appl. Phys. Lett.* **2011**, *99*, 113512. [\[CrossRef\]](#)
10. Kale, A.S.; Nemeth, W.; Guthrey, H.; Kennedy, E.; Norman, A.G.; Page, M.; Al-Jassim, M.; Young, D.L.; Agarwal, S.; Stradins, P. Understanding the charge transport mechanisms through ultrathin SiO<sub>x</sub> layers in passivated contacts for high-efficiency silicon solar cells. *Appl. Phys. Lett.* **2019**, *114*, 083902. [\[CrossRef\]](#)
11. Talbot, E.; Larde', R.; Pareige, P.; Khomenkova, L.; Hijazi, K.; Gourbilleau, F. Nanoscale evidence of erbium clustering in Er-doped silicon-rich silica. *Nanoscale Res. Lett.* **2013**, *8*, 39. [\[CrossRef\]](#)
12. Voitovych, V.V.; Rudenko, R.M.; Yuchymchuk, V.O.; Voitovych, M.V.; Krasko, M.M.; Kolosiuk, A.G.; Povarchuk, V.Y.; Khachevich, I.M.; Rudenko, M.P. Effect of tin on structural transformations in the thin-film silicon suboxide matrix. *Ukr. J. Phys.* **2016**, *61*, 980. [\[CrossRef\]](#)

13. Michailovska, K.V.; Indutnyi, I.Z.; Shepeliavyi, P.E.; Sopinsky, M.V.; Dan'ko, V.A.; Yukhymchuk, V.O. Luminescent and Raman study of nanostructures formed upon annealing of  $\text{SiO}_x\text{:Sm}$  films. *Semicond. Phys. Quant. Electr. Optoelectr.* **2023**, *26*, 068. [[CrossRef](#)]
14. Kizjak, A.Y.; Evtukh, A.A.; Bratus, O.L.; Antonin, S.V.; Ievtukh, V.A.; Pylypova, O.V.; Fedotov, A.K. Electron transport through composite  $\text{SiO}_2(\text{Si})\&\text{Fe}_x\text{O}_y(\text{Fe})$  thin films containing Si and Fe nanoclusters. *J. Alloys Compd.* **2022**, *903*, 163892.
15. Evtukh, A.; Kizjak, A.; Bratus', O.; Voitovych, M.; Romanyuk, V.; Mamykin, S.; Antonin, S.; Muriy, Y.; Klymenko, V.; Sarikov, A. Structure and electrical conductivity of nanocomposite  $\text{SiO}_x\text{N}_y(\text{Si})$  and  $\text{SiAl}_z\text{O}_x\text{N}_y(\text{Si})$  films. *J. Alloys Compd.* **2023**, *960*, 170879. [[CrossRef](#)]
16. Garrido, B.; Lopez, M.; Perez-Rodriguez, A.; Garcia, C.; Pellegrino, P.; Ferre, R.; Moreno, J.A.; Morante, J.R.; Bonafos, C.; Carrada, M.; et al. Optical and electrical properties of Si-nanocrystals ion beam synthesized in  $\text{SiO}_2$ . *Nucl. Instr. Methods Phys. Res. B* **2004**, *216*, 213. [[CrossRef](#)]
17. You, L.; Heng, C.L.; Ma, S.Y.; Ma, Z.C.; Zong, W.H.; Wu, Z.; Qin, G.G. Precipitation and crystallization of nanometer Si clusters in annealed Si-rich  $\text{SiO}_2$  films. *J. Cryst. Growth* **2000**, *212*, 109. [[CrossRef](#)]
18. Perego, M.; Fanciulli, M.; Bonafos, C.; Cherkashin, N. Synthesis of mono and bi-layer of Si nanocrystals embedded in a dielectric matrix by e-beam evaporation of  $\text{SiO/SiO}_2$  thin films. *Mater. Sci. Eng. C* **2006**, *26*, 835. [[CrossRef](#)]
19. Haque, S.M.; De, R.; Prathap, C.; Srivastava, S.K.; Rao, K.D. E-beam evaporation of silicon: Native oxidation and quasicontinuous tailoring of optical properties. *Phys. Stat. Solidi A* **2021**, *218*, 2100299. [[CrossRef](#)]
20. Laube, J.; Gutsch, S.; Hiller, D.; Bruns, M.; Kübel, C.; Weiss, C.; Zacharias, M. Formation of size controlled silicon nanocrystals in nitrogen free silicon dioxide matrix prepared by plasma enhanced chemical vapor deposition. *J. Appl. Phys.* **2014**, *116*, 223501. [[CrossRef](#)]
21. Klingsporn, M.; Kirner, S.; Villringer, C.; Abou-Ras, D.; Costina, I.; Lehmann, M.; Stannowski, B. Resolving the nanostructure of plasma-enhanced chemical vapor deposited nanocrystalline  $\text{SiO}_x$  layers for application in solar cells. *J. Appl. Phys.* **2016**, *119*, 223104. [[CrossRef](#)]
22. Tomozeiu, N.; Van Faassen, E.E.; Arnoldbik, W.M.; Vredenberg, A.M.; Habraken, F.H.P.M. Structure of sputtered silicon suboxide single- and multi-layers. *Thin Solid Films* **2002**, *420–421*, 382–385. [[CrossRef](#)]
23. Kahler, U.; Hofmeister, H. Visible light emission from Si nanocrystalline composites via reactive evaporation of  $\text{SiO}$ . *Opt. Mater.* **2001**, *17*, 83. [[CrossRef](#)]
24. Sasaki, M.; Ehara, T. Silicon oxide thin films prepared by vacuum evaporation and sputtering using silicon monoxide. *J. Phys. Conf. Ser.* **2013**, *417*, 012028. [[CrossRef](#)]
25. Inokuma, T.; Wakayama, Y.; Muramoto, T.; Aoki, R.; Kurata, Y.; Hasegawa, S. Optical properties of Si clusters and Si nanocrystallites in high-temperature annealed  $\text{SiO}_x$  films. *J. Appl. Phys.* **1998**, *83*, 2228. [[CrossRef](#)]
26. Wakayama, Y.; Inokuma, T.; Hasegawa, S. Nanoscale structural investigation of Si crystallites grown from silicon suboxide films by thermal annealing. *J. Cryst. Growth* **1998**, *183*, 124. [[CrossRef](#)]
27. Comedi, D.; Zalloum, O.H.Y.; Irving, E.A.; Wojcik, J.; Roschuk, T.; Flynn, M.J.; Mascher, P. X-ray-diffraction study of crystalline Si nanocluster formation in annealed silicon-rich silicon oxides. *J. Appl. Phys.* **2006**, *99*, 023518. [[CrossRef](#)]
28. Maslova, N.E.; Antonovsky, A.A.; Zhigunov, D.M.; Timoshenko, V.Y.; Glebov, V.N.; Seminogov, V.N. Raman studies of silicon nanocrystals embedded in silicon suboxide layers. *Semiconductors* **2010**, *44*, 1040. [[CrossRef](#)]
29. Zacharias, M.; Heitmann, J.; Scholz, R.; Kahler, U.; Bläsing, M.S.J. Size-controlled highly luminescent silicon nanocrystals: A  $\text{SiO/SiO}_2$  superlattice approach. *Appl. Phys. Lett.* **2002**, *80*, 661. [[CrossRef](#)]
30. Hinds, B.J.; Wang, F.; Wolfe, D.M.; Hinkle, C.L.; Lucovsky, G. Investigation of postoxidation thermal treatments of Si/ $\text{SiO}_2$  interface in relationship to the kinetics of amorphous Si suboxide decomposition. *J. Vac. Sci. Technol. B* **1998**, *16*, 2171. [[CrossRef](#)]
31. Dan'ko, V.A.; Indutnyi, I.Z.; Lysenko, V.S.; Maidanchuk, I.Y.; Min'ko, V.I.; Nazarov, A.N.; Tkachenko, A.S.; Shepeliavyi, P.E. Kinetics of structural and phase transformations in thin  $\text{SiO}_x$  films in the course of a rapid thermal annealing. *Semiconductors* **2005**, *39*, 1197. [[CrossRef](#)]
32. Zhigunov, D.M.; Seminogov, V.N.; Timoshenko, V.Y.; Sokolov, V.I.; Glebov, V.N.; Malyutin, A.M.; Maslova, N.E.; Shalygina, O.A.; Dyakov, S.A.; Akhmanov, A.S.; et al. Effect of thermal annealing on structure and photoluminescence properties of silicon-rich silicon oxides. *Physica E* **2009**, *41*, 1006. [[CrossRef](#)]
33. Wang, M.; Yang, D.; Li, D.; Yuan, Z.; Que, D. Correlation between luminescence and structural evolution of Si-rich silicon oxide film annealed at different temperatures. *J. Appl. Phys.* **2007**, *101*, 103504. [[CrossRef](#)]
34. Lisovskyy, I.P.; Voitovich, M.V.; Sarikov, A.V.; Litovchenko, V.G.; Romanyuk, A.B.; Melnik, V.P.; Khatsevich, I.M.; Shepeliavyi, P.E. Transformation of the structure of silicon oxide during the formation of Si nanoinclusions under thermal annealings. *Ukr. J. Phys.* **2009**, *54*, 383.
35. Nagamori, M.; Boivin, J.-A.; Claveau, A. Gibbs free energies of formation of amorphous  $\text{Si}_2\text{O}_3$ ,  $\text{SiO}$  and  $\text{Si}_2\text{O}$ . *J. Non-Cryst. Solids* **1995**, *189*, 270. [[CrossRef](#)]
36. Schnurre, S.M.; Gröbner, J.; Schmid-Fetzer, R. Thermodynamics and phase stability in the Si-O system. *J. Non-Cryst. Solids* **2004**, *336*, 1. [[CrossRef](#)]
37. La Magna, A.; Nicotra, G.; Bongiorno, C.; Spinella, C.; Grimaldi, M.G.; Rimini, E.; Coffa, L.C.S. Role of the internal strain on the incomplete Si/ $\text{SiO}_2$  phase separation in substoichiometric silicon oxide films. *Appl. Phys. Lett.* **2007**, *90*, 183101. [[CrossRef](#)]

38. Sarikov, A.; Zacharias, M. Gibbs free energy and equilibrium states in the Si/Si oxide systems. *J. Phys. Cond. Matter* **2012**, *24*, 385403. [[CrossRef](#)]
39. Sarikov, A. Internal strain mechanism of the incomplete phase separation of nonstoichiometric silicon oxide films. *Solid State Commun.* **2014**, *179*, 39. [[CrossRef](#)]
40. Sarikov, A. Mechanisms of the phase separation of nonstoichiometric Si oxide films: What can one learn from thermodynamics? *Proc. NAP* **2014**, *3*, 01NTF16.
41. Lisovskiy, I.P.; Sarikov, A.V.; Sypko, M.I. *Thin Film Structures with Silicon NanoInclusions*; Knigi-XXI: Kyiv-Chernivtsi, Ukraine, 2014; Available online: <https://www.books-xxi.com.ua/> (accessed on 25 January 2023). (In Ukrainian)
42. Sarikov, A. Thermodynamic study of the phase separation mechanisms in nonstoichiometric Si oxide films during high temperature annealing. In *Nanomaterials and Nanotechnology*; Ahmed, W., Ed.; One Central Press Ltd.: London, UK, 2016; pp. 58–73.
43. Sarikov, A. Crystallization behavior of amorphous Si nano inclusions embedded in silicon oxide matrix. *Phys. Stat. Solidi A* **2020**, *217*, 1900513. [[CrossRef](#)]
44. Sarikov, A.; Lisovskyy, I. Spinodal decomposition versus nucleation and growth mechanism of phase separation in nonstoichiometric silicon oxide films during high temperature annealing. *Solid State Commun.* **2019**, *287*, 19. [[CrossRef](#)]
45. Zelenina, A.; Sarikov, A.; Zhigunov, D.M.; Weiss, C.; Zakharov, N.; Werner, P.; López-Conesa, L.; Estradé, S.; Peiró, F.; Dyakov, S.A.; et al. Silicon nanocrystals in SiN<sub>x</sub>/SiO<sub>2</sub> hetero-superlattices: The loss of size control after thermal annealing. *J. Appl. Phys.* **2014**, *115*, 244304. [[CrossRef](#)]
46. Zelenina, A.; Sarikov, A.; Gutsch, S.; Zakharov, N.; Werner, P.; Reichert, A.; Weiss, C.; Zacharias, M. Formation of size-controlled and luminescent Si nanocrystals from SiO<sub>x</sub>N<sub>y</sub>/Si<sub>3</sub>N<sub>4</sub> hetero-superlattices. *J. Appl. Phys.* **2015**, *117*, 175303. [[CrossRef](#)]
47. Zhigunov, D.M.; Sarikov, A.; Chesnokov, Y.M.; Vasiliev, A.L.; Zakharov, N.; Kashkarov, P.K. Thickness and temperature depending intermixing of SiO<sub>x</sub>/SiO<sub>2</sub> and SiO<sub>x</sub>N<sub>y</sub>/SiO<sub>2</sub> superlattices: Experimental observation and thermodynamic modeling. *Appl. Phys. Lett.* **2016**, *108*, 223102. [[CrossRef](#)]
48. Zhigunov, D.M.; Sarikov, A.; Chesnokov, Y.M.; Vasiliev, A.L.; Zakharov, N.; Kashkarov, P.K. Response to “Comment on “Thickness and temperature depending intermixing of SiO<sub>x</sub>/SiO<sub>2</sub> and SiO<sub>x</sub>N<sub>y</sub>/SiO<sub>2</sub> superlattices: Experimental observation and thermodynamic modelling””. [*Appl. Phys. Lett.* *109*, 166101 (2016)]. *Appl. Phys. Lett.* **2016**, *109*, 166102. [[CrossRef](#)]
49. Sarikov, A.; Zhigunov, D. Thermodynamic mechanism of the intermixing of multilayered structures in the SiO<sub>x</sub>/SiO<sub>2</sub> superlattices with nanometer thick layers. *Mater. Today Commun.* **2017**, *13*, 163–169. [[CrossRef](#)]
50. Lisovskyy, I.P.; Voitovych, M.V.; Zlobin, S.O.; Lukianov, A.N.; Oberemok, O.S.; Dubikovskiy, O.V.; Sarikov, A.V. Infrared study of the structure of silicon oxynitride films produced by plasma enhanced chemical vapor deposition. *J. Non-Cryst. Solids* **2023**, under revision.
51. Nast, O. The Aluminium-Induced Layer Exchange Forming Polycrystalline Silicon on Glass for Thin-Film Solar Cells. Ph.D. Thesis, Philipps-Universität Marburg, Marburg, Germany, 2000.
52. Donovan, E.P.; Spaepen, F.; Poate, J.M.; Jacobson, D.C. Homogeneous and interfacial heat releases in amorphous silicon. *Appl. Phys. Lett.* **1989**, *55*, 1516. [[CrossRef](#)]
53. Spinella, C.; Lombardo, S.; Priolo, F. Crystal grain nucleation in amorphous silicon. *J. Appl. Phys.* **1998**, *84*, 5383. [[CrossRef](#)]
54. Porter, D.A.; Easterling, K.E. *Phase Transformations in Metals and Alloys*, 2nd ed.; CRC Press: Boca Raton, FL, USA, 2009.
55. Bongiorno, A.; Pasquarello, A. Validity of the bond-energy picture for the energetics at Si–SiO<sub>2</sub> interfaces. *Phys. Rev. B* **2000**, *62*, R16326. [[CrossRef](#)]
56. Philipp, H.R. Optical properties of non-crystalline Si, SiO, SiO<sub>x</sub> and SiO<sub>2</sub>. *J. Phys. Chem. Solids* **1971**, *32*, 1935. [[CrossRef](#)]
57. Winer, K. Defect formation in a-Si:H. *Phys. Rev. B* **1990**, *41*, 12150. [[CrossRef](#)] [[PubMed](#)]
58. Boninelli, S.; Iacona, F.; Franzò, G.; Bongiorno, C.; Spinella, C.; Priolo, F. Formation, evolution and photoluminescence properties of Si nanoclusters. *J. Phys. Cond. Matter* **2007**, *19*, 225003. [[CrossRef](#)]
59. Roussel, M.; Talbot, E.; Pareige, P.; Gourbilleau, F. Influence of the supersaturation on Si diffusion and growth of Si nanoparticles in silicon-rich silica. *J. Appl. Phys.* **2013**, *113*, 063519. [[CrossRef](#)]
60. Vanhellemont, J.; Claeys, C. A theoretical study of the critical radius of precipitates and its application to silicon oxide in silicon. *J. Appl. Phys.* **1987**, *62*, 3960. [[CrossRef](#)]
61. Borghesi, A.; Pivac, B.; Sassella, A.; Stella, A. Oxygen precipitation in silicon. *J. Appl. Phys.* **1995**, *77*, 4169. [[CrossRef](#)]
62. Magomedov, M. Dependence of the surface energy on the size and shape of a nanocrystal. *Phys. Solid. State* **2004**, *46*, 954. [[CrossRef](#)]
63. Lu, H.M.; Jiang, Q. Size-dependent surface energies of nanocrystals. *J. Phys. Chem.* **2004**, *108*, 5617. [[CrossRef](#)]
64. Zacharias, M.; Streitenberger, P. Crystallization of amorphous superlattices in the limit of ultrathin films with oxide interfaces. *Phys. Rev. B* **2000**, *62*, 8391. [[CrossRef](#)]
65. Peibst, R.; Dürkop, T.; Bugiel, E.; Fissel, A.; Costina, I.; Hofmann, K.R. Driving mechanisms for the formation of nanocrystals by annealing of ultrathin Ge layers in SiO<sub>2</sub>. *Phys. Rev. B* **2009**, *79*, 195316. [[CrossRef](#)]
66. Lisovskyy, I.P.; Indutnyy, I.Z.; Gnenny, B.N.; Lytvyn, P.M.; Mazunov, D.O.; Oberemok, A.S.; Sopinskyy, N.V.; Shepelyavyi, P.E. Structural-phase transformations in SiO<sub>x</sub> films in the course of vacuum heat treatment. *Semiconductors* **2003**, *37*, 97. [[CrossRef](#)]

67. Sarikov, A.; Litovchenko, V.; Lisovskyy, I.; Maidanchuk, I.; Zlobin, S. Role of oxygen migration in the kinetics of the phase separation of nonstoichiometric silicon oxide films during high-temperature annealing. *Appl. Phys. Lett.* **2007**, *91*, 133109. [[CrossRef](#)]
68. Sarikov, A. Kinetic model of precipitate growth during phase separation in metastable binary solid solutions. *Solid State Phenom.* **2016**, *242*, 196. [[CrossRef](#)]
69. Van Hapert, J.J.; Vredenberg, A.M.; van Faassen, E.E.; Tomozeiu, N.; Arnoldbik, W.M.; Habraken, F.H.P.M. Role of spinodal decomposition in the structure of SiO<sub>x</sub>. *Phys. Rev. B* **2004**, *69*, 245202. [[CrossRef](#)]
70. Pivot, J. Mechanical properties of SiO<sub>x</sub> thin films. *Thin Solid Films* **1982**, *89*, 175. [[CrossRef](#)]
71. Sze, S.M. *Physics of Semiconductor Devices*, 2nd ed.; John Wiley & Sons: New York, NY, USA, 1981.
72. Wortman, J.J.; Evans, R.A. Young's modulus, shear modulus, and Poisson's ratio in silicon and germanium. *J. Appl. Phys.* **1965**, *36*, 153. [[CrossRef](#)]
73. Lucovsky, G.; Phillips, J.C. Bond strain and defects at Si–SiO<sub>2</sub> and internal dielectric interfaces in high-k gate stacks. *J. Phys. Condens. Matter.* **2004**, *16*, S5139. [[CrossRef](#)]
74. Yi, L.X.; Heitmann, J.; Scholz, R.; Zacharias, M. Si rings, Si clusters, and Si nanocrystals—Different states of ultrathin SiO<sub>x</sub> layers. *Appl. Phys. Lett.* **2002**, *81*, 4248. [[CrossRef](#)]
75. Zhang, W.; Zhang, S.; Liu, Y.; Chen, T. Evolution of Si suboxides into Si nanocrystals during rapid thermal annealing as revealed by XPS and Raman studies. *J. Cryst. Growth* **2009**, *311*, 1296. [[CrossRef](#)]
76. Hernández, S.; Martínez, A.; Pellegrino, P.; Lebour, Y.; Garrido, B.; Jordana, E.; Fedeli, J.M. Silicon nanocluster crystallization in SiO<sub>x</sub> films studied by Raman scattering. *J. Appl. Phys.* **2008**, *104*, 144304. [[CrossRef](#)]

**Disclaimer/Publisher's Note:** The statements, opinions and data contained in all publications are solely those of the individual author(s) and contributor(s) and not of MDPI and/or the editor(s). MDPI and/or the editor(s) disclaim responsibility for any injury to people or property resulting from any ideas, methods, instructions or products referred to in the content.